Tampere University

Ahmed Elsayes

ARTIFICIAL SKIN WITH SENSE OF TOUCH FOR ROBOTIC HAND

Faculty of Engineering and
Natural Sciences
Master of Science thesis
4th July 2019

ABSTRACT

Ahmed Elsayes: Artificial skin with sense of touch for robotic hand
Master of Science Thesis
Tampere University
Master's Degree Program in Automation Engineering
July 2019

This Master of Science thesis proposes a method to fabricate a soft robotic hand (SRH) with a sense of touch. Electronic skin (e-skin) – flexible and/or stretchable electronics that mimic the functions of human skin – is actively researched and developed for robotic applications (especially humanoid robots), owing to the high demand of robots that can safely interact with humans in the different industrial sectors. E-skin is also in demand for high-quality prosthetics that leverage the advances in brain-machine interfaces.

The emphasis in this thesis is on the fabrication and characterization of an e-skin. The objective of this skin is to give an estimation of the amount of force exerted on it, which is beneficial for the SRH to feedback information about the manipulated object.

We are aiming in this thesis to use fabrication approach of rapid prototyping to fulfill the following characteristics in SRH: actuation, soft touch, and sensation capabilities. Accordingly, we propose using 3D printing to fabricate both hand skeleton and molds to be used for artificial skin casting. Fingers are actuated by driving cables which are extended through inner channels embedded inside the hand skeleton.

The specific goal of this thesis is to compare two different types of touch sensors for e-skin, one piezoresistive and one capacitive. The selected technologies are discussed in detail, and sensors based on these technologies are fabricated, characterized and analyzed comparatively. The results showed the potential of disclosing tactile information by implanting sensors in SRH. With comparing the piezoresistive sensor to the capacitive sensor, the latter exhibited a simpler approach for integration with the artificial skin to develop e-skin because it was feasible to fabricate the e-skin in one step instead of fabricating the artificial skin and the sensor separately. From the perspective of performance, capacitive sensor demonstrated higher efficiency in general compared to the piezoresistive sensor. As an example, the response in the piezoresistive and capacitive sensor, showed linearity of 5.3% (on a logarithmic scale) 1.8% for both sensors, respectively. Moreover, the signal hysteresis in the capacitive sensor was better with a deviation of 2.7%, compared to 18.2% for the piezoresistive sensor.

Finally, a SRH with integrated touch sensors is demonstrated. This paves the way for further research on utilizing the developed e-skin for objects recognition during hand gripping or designing a closed control loop system for dexterous control over the force of gripping. Moreover, an efficient artificial limb with sensation capabilities can be developed to feedback sensory information to the brain of the patient after being processed by a brain-machine interface.

Keywords: Soft Robotic Hand, Prosthetics, Brain-Machine Interface, Additive manufacturing, 3D printing, Tactile sensor, Piezoresistive sensor, Capacitive sensor, Electronic Skin

PREFACE

This thesis work came to mark an end for an important chapter in my life and provide me with the chance to plan for another chapter. To finish this work, I needed patience, persistence and support of people around me.

First, I would like to express my deep gratitude to my supervisor Assistant Professor Veikko Sariola, who was following up my progress regularly and guiding me along this journey. I learned a lot from him during this experience. I cannot find any words that express my gratitude to doctoral researcher Anastasia Koivikko, who encouraged me to start early, trained me on many tools needed in my research and followed up my progress. I want also to express my thanks to Assistant Professor Roel Pieters who accepted to supervise my work. I cannot also forget to give the credit to doctoral researcher Nur-E-Habbiba for her guidance on my thesis writing and Dr. Vipul Sharma for his encouragement to me.

Finally, I owe to my parents in unpayable debt on their support to me to bypass all obstacles. They lived every moment of fail and success with me since I completed the bachelor's degree until I finished my thesis for a master's degree. Their prayers opened the doors for me and introduced me to wonderful people. They were always supporting me to bypass all hardships and I will never disappoint their expectations in me.

Tampere, 4 July 2019

Ahmed Elsayes

CONTENTS

LIST OF SYMBOLS AND ABBREVIATIONS

CAD	Computer-Aided Design
CAM	Computer-Aided Manufacturing
CNT	Carbon Nanotube
DAQ	Data Acquisition
e-skin	Electronic skin
FDM	Fused Deposition Modeling
IC	Integrated Circuit
LOD	Limit Of Detection
MIG	Micro-structured ionic gel
PDMS	PolyDiMethylSiloxane
PET	Polyethylene terephthalate
PLA	Polylactic acid
PVDF	Polyvinylidene fluoride
SLA	Stereolithography
SNR	Signal to Noise Ratio
SRH	Soft Robotic Hand
STL	Standard Tessellation Language

A	Area
C	Capacitance
Cf	Constant associated with edges of the electrode in the capacitive sensor
d	Distance between conductive plates
L	Length
m	loading variable in grams
P	Input signal of the sensor
R	Resistance
t	Time variable
Vs	Supply voltage
Vo	Voltage across the passive resistor
Vc	Voltage across the capacitor
X	Output signal of the sensor
ρ	Resistivity
εr	Relative dielectric constant
εo	Electric Permittivity of the vacuum
$\bar{x}$	Mean of the signal
σ	Standard deviation

1. INTRODUCTION

1.1 Overview

Developing versatile robotic and prosthetic grippers are attracting a lot of attention. The robotic grippers are demanded in industrial applications by integration in the production lines to automate the production. Additionally, prosthetic grippers are needed in biomedical applications to grant the amputee the ability of interaction with the surrounding objects by implanting artificial limbs that mimic the functionalities of his/her lost natural limbs. A few decades ago, the idea of rapid prototyping grippers with capabilities comparable to the human hand in terms of sensation, the softness of touch, dexterous manipulation and biocompatibility was in the realms of science fiction. However, thanks to rapid progress in material science, sensation technologies, Computer-Aided Design (CAD) and Computer-Aided Manufacturing (CAM); humanoid robots, which are mimicking many human functions, have become a reality [1]–[3].

Soft grippers are of interest to many researchers and industrialists owing to the escalated need for automatization. The rapid progress towards automation and the need to create an environment for robots and humans to interact safely stimulated the interest in these grippers, especially, in plants where soft assets are needed to handle tasks that governed by strict health and safety regulations. As an example, for many decades food industry was one of the heavy labor industries, however, some companies (e.g. Softrobotics, United States [4]) offer soft grippers that serve food and beverages industry. To clarify, the company demonstrated many cases for utilizing these grippers in automating the production lines to handle the delicate food items, even under the conditions of high-speed processing. From expenses perspective, the cost of robotic hands can also be high: [5] in biomedical applications, the latest developed bionic hand with a soft touch can cost 50,000 dollars (Mobius Bionics, United States [6]). In addition to the contribution of the sophisticated characteristics of these prosthetics in defining the price, the exterior appearance and soft touch attributes play a deterministic role in increasing the price of these prosthetics, as the amputees in major cases want to possess artificial limbs that mimic the functionalities and resemble the normal limbs.

High progress is achieved in the domain of prosthetics design, techniques of activation and the success in developing a reliable approach for actuating artificial limbs by decoding the electroencephalographic signals (signals that are collected from sensors that attached to specific muscles along the arm) [7]. However, there is still a lack of conducted research in the domain of stretchable tactile sensors that is compliant with a soft prosthetic hand. The successful research in the domain of brain-machine interfaces facilitated both unidirectional and bidirectional control of the prosthesis. Unidirectional control is about supplying the gripper with signals that extracted myoelectrically from muscles without feeding back any sensory information from the prosthesis. On the other hand, bidirectionally control is about commanding the prosthesis by decoding amputee's intentions and restoring the human sensation by implanting specific sensors in the prosthetics to deliver sensory feedback to the brain [8]. Consequently, the amputee can effectively modulate the gripping force without the need for visual or auditory observation (Figure 1), which is physiologically plausible for the patient, as it would give him/her the sense of possessing semi-natural hand. Moreover, whether the hand with sensory apparatus is defined to be used as prosthetics or robotic hand for industrial applications, the successful implementation of tactile sensors in the gripper could result in feeding back information about shape, size or stiffness of the targeted objects.

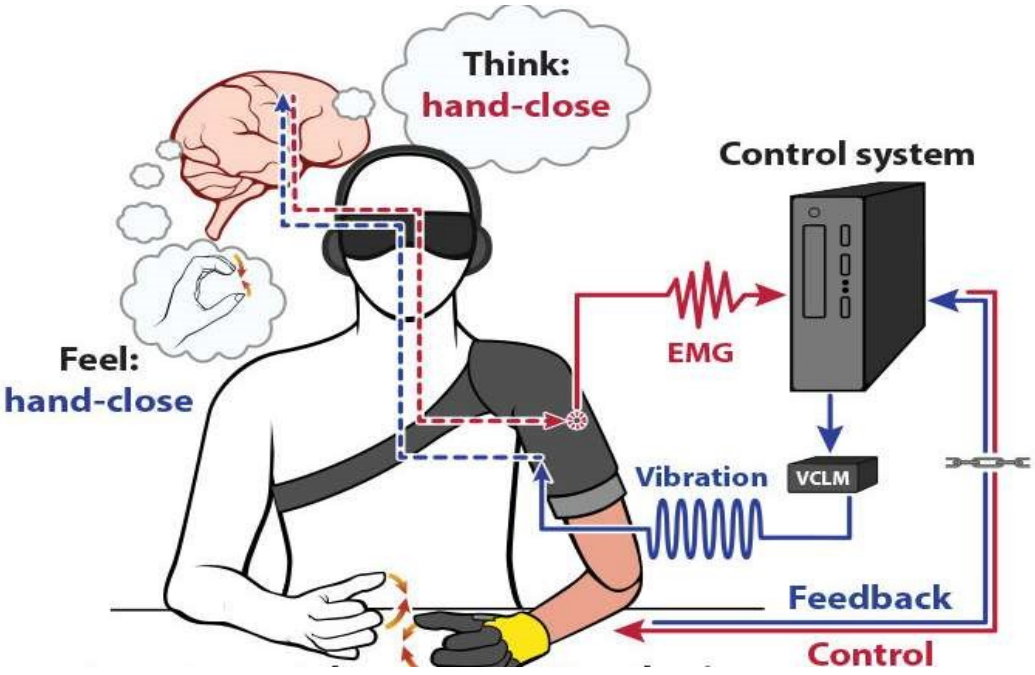

Figure 1. *Schematic description for the bidirectional control to command the prosthetic hand and retrieve sensory information from it* [9]

1.2 Objective

The overall objective in this thesis is to fabricate a robotic hand inspired by human hand, with the following requirements: dexterous manipulation, soft touch and tactile sensation. Here, dexterous manipulation is taken to mean the ability of the gripper to manipulate a variety of objects with different geometries. In general, the number of degrees of freedom (DOF) dictates the dexterity of the gripper. By increasing the DOF, a higher dexterity is achievable. Regarding soft touch capability, it means the ability of the gripper to absorb mechanical shocks, or in other words, the gripper exhibits a higher range of compressibility. Whereas, this can be achieved by using a material with high elasticity.

Consequently, we needed to work on these three components: the artificial skeleton, the artificial skin and the tactile sensor. The skeleton gives the gripper the shape and dexterity it needs for manipulating objects. Therefore, it should be designed to ensure an adequate number of DOF without increasing the complexity of the overall design. The artificial skin should be synthesized from polysiloxane rubber to grant the gripper the desired attribute of soft touchiness. The tactile sensor allows some level of interaction with the surrounding environment because it can convert physical quantities (pressure, force) into a measurable signal [1], [10]–[12].

All these three components of the gripper will be discussed in terms of the techniques of fabrication, methodology, designs, and the results will be discussed in this thesis. However, the specific objective of the thesis is to characterize two different tactile sensors. To decide on which two technologies should be chosen, we need to know that the sensor selection is application-driven. Therefore, this thesis will focus on finding a sensor, which can detect load exerted on the Soft Robotic Hand (SRH**).** Generally, there are numerous technologies that can be utilized to produce flexible tactile sensors such as resistive, piezoresistive, capacitive, piezoelectric and optoelectrical technologies. This thesis will review and compare these technologies by explaining the advantages and disadvantages related to each technology in terms of the desired attributes of low cost, simplicity, and sensitivity. However, compatibility with the targeted application in terms of flexibility (and stretchability in some cases) are also crucial attribute for the synthetic sensor. Accordingly, a capacitive and a piezoresistive will be fabricated and compared to evaluate their suitability for this application. It is worth mentioning that many factors are involved in the process and many techniques can be elaborated for satisfying the previously mentioned goals for such a dexterous gripper. The thesis aims at answering the following research questions:

1. What rapid prototyping method can be used to fabricate the skeleton, the skin and the sensors that could allow reconfigurability and pave the way for democratizing the production of such robotic hands?

2. What are the key performance characteristics of the two specific sensors chosen for the study, such as linearity, drift, sensitivity, signal-to-noise-ratio and applicability for integration in electronic skin (e-skin)? How do the two sensors compare to each other?

1.3 Outline

The thesis is divided in the following manner:

Chapter 1 presents an overview about the topic of the thesis, elevating the motivation through describing the importance of research in this topic.

Chapter 2 provides an overview of the latest advances in the domain of bionics in terms of various proposals for both artificial skin and artificial skeleton design, fabrication approaches and the standards for an efficient human-inspired robotic hand.

Chapter 3 provides an overview of the technologies used in the synthesis of flexible tactile sensors and reasoning the selectively chosen technologies to be studied comparatively for sensor fabrication.

Chapter 4 shows the mechanical design and the fabrication approach for both of artificial skeleton and artificial skin, respectively; furthermore, the materials for artificial skin will be highlighted to give hint about the preferred characteristics and reasoning the selection of specific material in the different phases.

Chapter 5 introduces the two selected technologies that will be used for tactile sensation, highlighting the proposed design for the sensors, the approach of fabrication and the potential of integration with the SRH.

Chapter 6 demonstrate the elaborated instruments for testing characterizing the fabricated sensors, explaining the hardware configuration for both sensors.

Chapter 7 compares the performance of the two fabricated sensors under different forms of loads. Demonstrating the actuation of the hand and the stimulated response in the e-skin after selectively choosing one of the two sensors for the demonstration case.

Chapter 8 contains the discussion on the results and highlighting the potential future work

Chapter 9 concludes the thesis.

2. LATEST ADVANCES IN BIONICS

This chapter gives an overview of the latest advances in bionics. First, the concepts behind the mechanisms for prosthesis are reviewed. Then, different fabrication approaches for prosthetics are analyzed. Finally, the chapter gives an overview of the standard approach to fabricate artificial skin, the desired attributes of the artificial skin and the basis of selecting the material that is involved in the synthesis process.

2.1 Artificial skeletons

The work on developing a dexterous robotic hand had started decades ago, driven by the demand for utilization in the industry [13] and space exploration [14]. In industry, the ultimate goal was to develop humanoid robots with the ability to manipulate the targeted objects. As a matter of fact, the racing for space exploration was the highest stimulus for inciting the interest in developing dexterous robotic hand [15]. Nevertheless, the first principles for achieving dexterity in the robotic hand with hard finger components (non-rolling and non-sliding) was presented in Salisbury work (1985) [16]. The hypothesis simply stated that nine DOF is the minimum number that assures the dexterity in the hand innervated by rigid components. Accordingly, other researchers started to develop similar design schemes by considering the implication of three joints per each finger in the robotic hand, such as the hand developed in University of Karlsruhe [17], Delft University [18] and Technical University of Darmstadt [19].

However, the development of the Utah/MIT hand [20] demonstrated a leap toward elevating the attention in the design of anthropomorphic robotic hand because it was closely mimicking the outer appearance of the human hand. The hand had 16 DOF, actuated by tendons and pneumatic actuators. While, the focus in research during this period was on developing a robotic hand (either entirely soft or anthropomorphic) that actuated by electric motors and tendons [20], [21] or pneumatic actuators [22]; Shape Memory Alloy (SMA) is proposed in Hitachi Hand as a mechanism for hand actuation [23]. The SMA-driven hand distinguished by the high power to weight ratio. Each SMA wire had a small diameter up to 0.02 mm. Initially, the hand articulated components are straightened by attached springs. The hand fingers were commanded to bend by heating the SMA wires through passing an electrical current in it. To clarify, The SMA has a property of contraction in response to variation of inner temperature of SMA when it heated up beyond a specific threshold. The force of contraction that was generated by the SMA is opposing

the force of expansion that was generated by the spring, which allows controllability over hand fingers to actuate it bidirectional by passing electrical current into the SMA wires.

Later, Hirzinger *et al.* [24] proposed a multisensory four-finger hand with 12 DOF to be utilized for space operations. The target was to integrate all the actuators in the hand, which increased the complexity of the hand. Despite the interesting results that produced in these past decades, the complexity of these robotic hands was high as it was heavily relying on mechanically interconnected components, gearboxes and metallic rigid appearance.

Due to the recent progress in material sciences, and the introduction of technologies such as CAD and CAM, researchers were able to propose dozens of different designs for hand exoskeletons [2] that can be prototyped in a simple manner. By considering the level of complexity and functionalities of the robotic hand, we will limit our analysis to two designs; the first is a tendon-driven robot hand, and the second is a modular hand with an integrated drive system where the joints are driven directly by the actuators. Figure 2 shows a 3D printed skeleton for a whole hand with an environmentally sensitive soft touch (a) and the detailed structure for one finger (b).

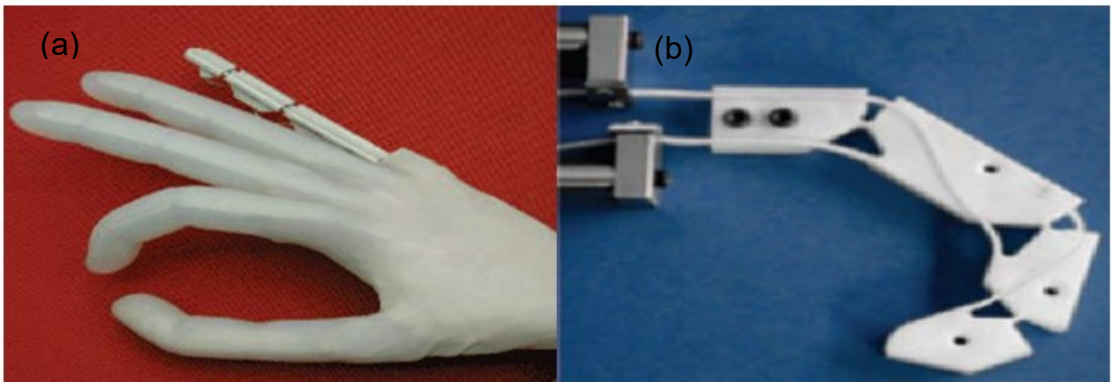

Figure 2. *(a) Endoskeleton principle interacting physically with the environment. The image shows the entire hand structure after components assembly and enfolding the 3D printed structure inside an elastomeric material (b) Tendon-driven finger. The image shows a bending response by pulling the cable that connects the finger phalanges [2]*

The tendon-driven robot hand employs the twisted-string actuation mechanism to drive the free-moving components of the hand. Many joint types have been reported in the literature such as pulley-based finger design [25], compliant joints that act as notch hinges, close-wound springs to form a different type of compliant joints [2] and flexural hinges that deform elastically to incite a compliant articulation [25] (Figure 3). Nevertheless, a preferred solution is one, which ensures simplicity, durability, and compliance with the sensory apparatus. A rotational compliant joint based on pin and ball principles will

be adequate to satisfy these attributes because they allow rotation for the articulated endoskeletal structures and allow the joints to snap into place, which guarantees the smoothness of any rotation around the perpendicular axis of extremities. In addition, the design of the tendon-driven hand facilitates assembly and disassembly of the articulated components quickly.

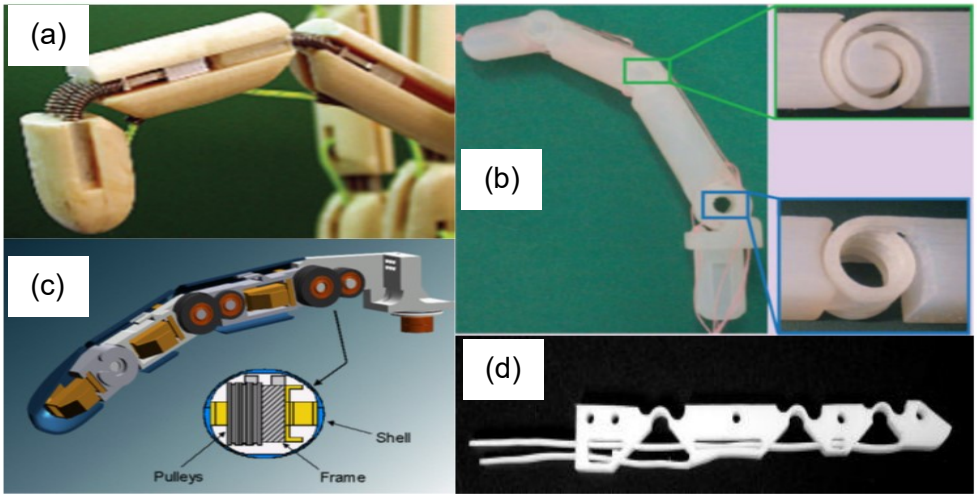

Figure 3. *Different types of joint utilized in tendon driven- based robotic hand such as notch hinges [2], close-wound springs [2], pulley-based finger design* [25]*, flexural hinges* [25]

The modular hand utilizes an integrated system to drive the joints. Naturally, these are much more complex structures than the tendon-driven robot hand because the actuators, sensors, connectors and electronic chips all have to be placed in the same robotic hand, in contrast to the first type, where, driving tendons, which are guided through paths integrated within the finger, can actuate joints remotely. The integrated type has certain attributes, such as robustness, but it is highly complex and expensive to manufacture, which make it a reasonable choice for heavy applications in industry that require robust gripper with precise control over the end-effector, but a poor choice if it is intended to be used in bionics or to maneuver light loads in the industry.

2.2 Fabrication approaches for rigid objects

3D printing (also known as additive manufacturing) [26] is a technology used to create 3D objects by slicing these objects into contiguous 2D layers and printing them layer-by-layer.

The revolution in 3D printing combined with the trend toward opening the sources behind these technologies has facilitated the rapid and easy prototyping of almost any structure that can fit the size of the printer. There are many 3D printing technologies, such as stereolithography (SLA), digital light processing, fused deposition modeling (FDM), selective laser sintering, electronic beam melting and laminated object manufacturing [27].

At the laboratory where this thesis work was carried out, only two of these methods were readily available – SLA and FDM – so these two methods were used in the fabrication of the robotic hand and thus only these two will be discussed in detail.

To get the 3D object printed, both FDM and SLA technologies need CAD files to produce the object. This file contains information about the dimensions of the object. Before it can be uploaded to the printer, the CAD file needs to be converted to another format called Standard Tessellation Language (STL). This format is understandable by the 3D printer, which slices the CAD design into layers along its Z-axis. Every layer thus has the necessary information for translation into displacement commands for the actuators of the X-axis and Y-axis [26].

The principle of operation of SLA depends on utilizing the laser beam to be directed to photosensitive polymer where the laser is directed according to the instructions generated based on the CAD file. In every spot covered by the laser beam, the photosensitive polymer is converted into a solid 3D object. This process continues layer by layer as a platform, which is initially in contact with the liquid plastic, moves along the Z-axis until each layer is completed in order to process the next layer. The process continues until all the layers have been completed, and the 3D object is ready [26]. Finally, in a complementary step to acquire high quality objects, the printed object is rinsed in isopropanol to ensure removal of monomer and any residual impurities on the object. Thereupon, the object can be cured by exposure to ultraviolet light for a specific period of time according to the specifications of the utilized resin [28].

The operation principle of FDM relies on the same layer-by-layer printing; however, unlike with the SLA technique, FDM technique utilizes a thermoplastic filament instead of liquid plastic. Commonly, the printer has a Cartesian structure to enable it to operate along the X, Y and Z-axes. Nozzle extruder reinforced with heater is utilized to melt the thermoplastic filament and propel it out of the nozzle. The propelled plastic forms a thin layer of plastic while the stage is moving along X and Y-axis. Every printed layer binds to the layer beneath it, once the plastic cools down [26].

A FDM printed object needs supporting pillars to avoid the collapse of the object and ensure the separation between the object and the workspace plate. The usual solution

to separate the object from workspace is to place a special material underneath the printed object at the beginning of the printing process. This material can be dissolved by an appropriate solvent and removed mechanically after the completion of printing [26].

2.3 Fabrication approaches for soft robotic skin

To fabricate a soft artificial skin for a robotic device, elastomer casting is often been used [29]. Elastomer casting is a technique of using an elastomeric material and a replica mold to replicate a specific structure. Typically, the elastomer material is a polysiloxane-based organic polymer with specific characteristics such as skin-like softness, high elongation at break (what the maximum strain that can happen in the polymer before it breaks permanently), high thermal stability, chemically inert and low toxicity.

Generally, the elastomer casting process is performed according to the following steps:

1. Mold fabrication, which works as a stamp for replicating structures made of the elastomer. The mold can be fabricated by any technology of additive manufacturing and material of the mold can be selected according to the targeted application.

2. Typically, the elastomer exists preliminary in two separated materials in liquid form. The two material are mixed carefully to ensure the cross-linking. The mixing process can be performed manually or by using a centrifugal mixer; however, based on experimental observations, centrifuging the mixture ensures better cross-linking.

3. Pouring the mixture inside the mold.

4. Optionally, degassing the mixture inside a vacuum a chamber; this process allows the extraction of air bubbles from the mixture, which reflects positively on the quality of elastomer.

5. Leaving the mixture inside the mold for long hours to get the elastomer solidified in the room temperature, or heating it in the oven, whereas adopting any of these two options renders to the elastomer specifications and the targeted application for it.

There are many types of polysiloxane elastomers with different characteristics, and the selection of the material is dependent on the application. In our application case, we need to concentrate on a material with considerably high elasticity and enough tensile strength to ensure durability while maintaining the soft touch of the robotic hand.

Typically, the elasticity of the material can be defined by Young's modulus (E), which represent the ratio of the stress (σ) exerted on the material to the strain (ε) induced in it in response to this stress.

$$E = \frac{\sigma}{\varepsilon} \tag{1}$$

The lower value of Young's modulus indicates higher elasticity that is realizable from the material.

To explain the selection of polysiloxane-based organic polymer as a material for artificial skin, Figure 4 demonstrates Young's modulus range of various types of soft materials. we can notice the proximity of polysiloxane elastomers to biological skins [30].

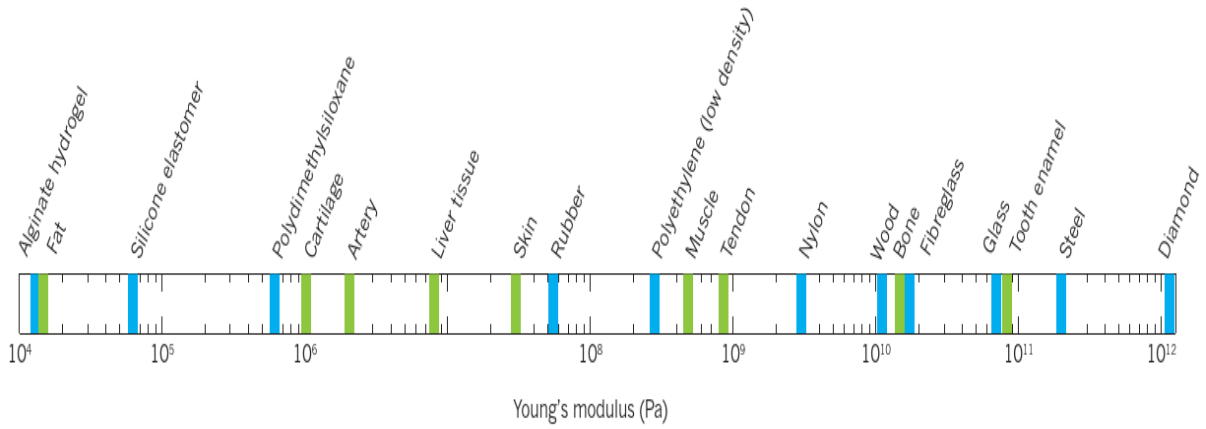

Figure 4. *Young's modulus for some of the synthetic and biological materials* [30]

Moreover, the comparative study [31] disclosed adequacy of polysiloxane elastomers for soft touch applications and also showed the availability of a broad range of elasticity that can be acquired by customizing the material based on the targeted specifications (Figure 5). As an example, there are many polysiloxane elastomers provided by SMOOTH-ON (U.S.A) [32] such as Ecoflex 00-10, Ecoflex 00-30, Ecoflex 00-50, Dragon Skin F/X PRO and Dragon Skin 20; where it is shown in Figure 5 how the elastomers can be highly customizable to fulfill specific requirements [31].

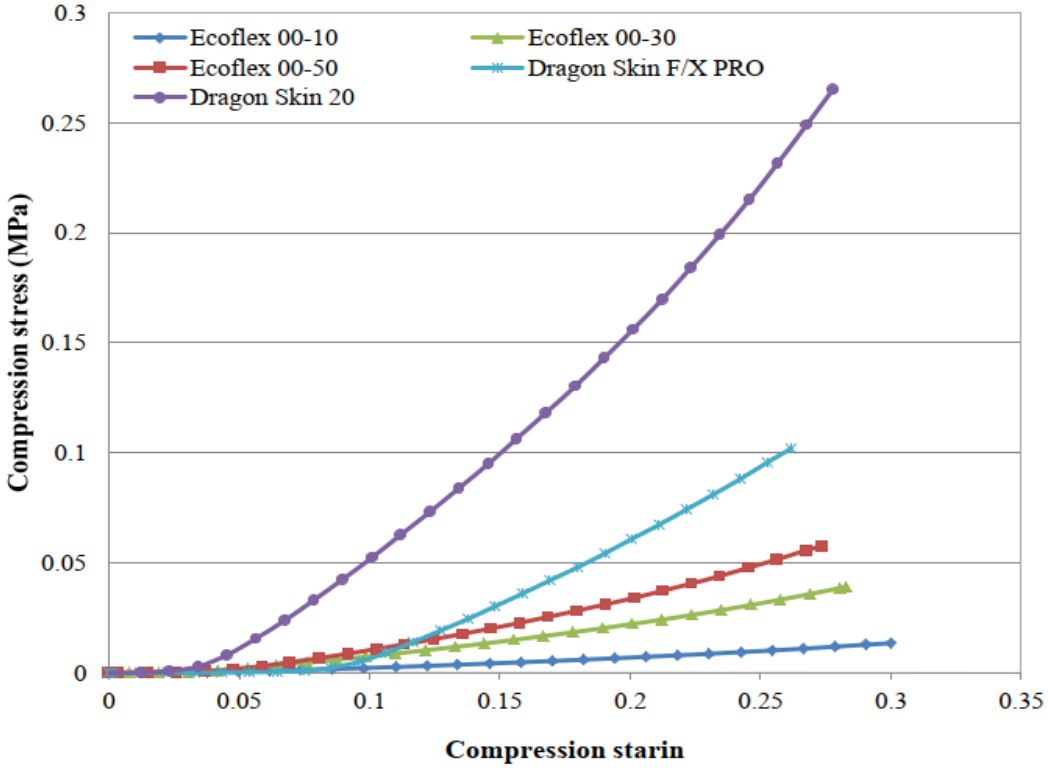

Figure 5. *The difference of Young's modulus for 5 elastomeric polymers, obtained by recording the strain ratio under different magnitudes of stress applied on the specimen* [31]

To point out, Young's modulus of Ecoflex 00-30 and Young's modulus of Dragon Skin 20 is found to be 0.1694 MPa and 1.1143 MPa [31], respectively. On the other hand, the normal skin of the human is found to be around 0.1012 MPa (the average with averting being hydrated or dehydrated) [33]. In conclusion, we can assume from these statistics that these synthetic elastomers can be used as alternatives for their biological counter-parts.

3. FLEXIBLE TACTILE SENSORS

This chapter gives an overview of flexible sensors and the technologies used in the synthesis of flexible tactile sensors, taking into consideration that we will limit the interest to the measurement of force applied to the sensor. Tactile sensors possess many attributes, such as stretchability, cost and ease of fabrication. The selection of the sensor is typically dictated by the target application. In this chapter, the advantages and disadvantages of different tactile sensors are reviewed.

However, before discussing the various technologies, we need to define the flexible sensor. The flexible sensor is a device with high mobility to be bent or twisted in different directions. The mechanism in the sensor works by converting a physical stimulus into an electrical signal. The type of electrical signal depends on the technology of the sensor.

The key parameters [3][11] that should be considered for evaluating the sensor:

1. Sensitivity, the property which reflects the measuring effect and accuracy of the sensor, Typical defined by $\Delta X/\Delta P$, whereas, X and P denote the quantitative output signal and the input (physical stimulus), respectively.
2. Limit of detection (LOD) is the parameter, which indicates the maximum and minimum value of the exerted stimuli to get a response from the sensor.
3. Hysteresis, the parameter that determines undesirable variation in the system response (output) when the input values are the same but performed from opposite directions. For instance, in the case of pressure sensor, the hysteresis range is estimated by measuring the value of sensor output (e.g. voltage) in response to input (e.g. first reading will be the pressure while it is increasing, and the second reading will be the pressure while it is decreasing in case of pressure sensor).
4. Drift, the parameter that estimates the maximum shift of output, while the constant value of the input (e.g. pressure in case of pressure sensor) is applied on the device.
5. Response time, the parameter that defines the time since the stimuli are applied until the sensor gives a stable output signal.
6. Signal to noise ratio (SNR), the parameter that determines the strength of the signal to be detected and eventually processed by measuring the ratio between the signal power to the noise power.
7. Creep effect, the parameter that indicates the tendency of the sensor to give a slow change in the output because of elastic or plastic deformation of the sensor, while it is under the effect of mechanical stimuli (e.g. stress, tension, torsion, etc.)

Other parameters to be considered for sensor evaluation, such as stability, repeatability, robustness, linearity, response and recovery time. The technology review in this chapter is based on reference [11] unless otherwise mentioned.

3.1 Resistive and piezoresistive type

The principles of operation in a resistive type sensor depends on the change of electrical resistance of the sensor in response to an external stimulus, such as pressure, bending or twisting that lead to sensor deformation. Typically, the sensors are designed with a specific shape to maximize its sensitivity to the physical stimulus of interest, which helps in obtaining an accurate estimation about the level of mechanical stimuli exerted on the sensor. Resistive type sensor is fabricated from conductive material patterned on a dielectric substrate. Commonly, the resistive sensor is manufactured as a strain gauge [34]. To clarify, the strain gauge is a metallic foil that is arranged in a zig-zag pattern and bonded to a non-conductive substrate called the carrier (Figure 6). This type of sensor is governed by the Poisson effect phenomenon, which measures the negative ratio of strain in the transverse direction to the strain in the axial direction when the material is under compression. Under mechanical compression, some level of strain is induced in the metallic foil, which leads correspondingly to a variation in the resistivity of it based on the following relation:

$$R = \rho \frac{L}{A}\,, \tag{1}$$

where R is the resistance, ρ is the resistivity of the metallic foil, L is the length of metallic foil, A is the cross-sectional area of the metallic foil. From equation (1), the rationale behind the zig-zag pattern can be understood: it maximizes the sensitivity of the sensor. Typically, the so-called gauge factor is used to estimate the sensitivity of the sensor to the strain. Gauge factor is the ratio of the fractional change in resistance (ΔR) to the fractional change in strain (ΔL):

$$GF = \frac{\Delta R/R}{\Delta L/L}. \tag{2}$$

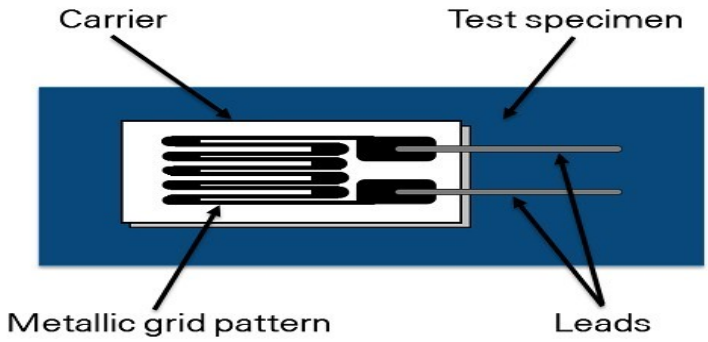

Figure 6. *Strain Gauge sensor to estimate the variation in electrical resistance proportional to strain induced by mechanical stimulus* [34]

As an example on a resistive sensor to estimate the degree of bending in a pressure-driven soft robot, Koivikko *et al.* [10] proposed the use of a screen printer to fabricate a resistive type sensor to measure the curvature of a soft actuator. A silver ink (ECM / CI-1036) was screen-printed on a 50 µm thick thermoplastic polyurethane substrate (Epurex1 Platilon / U4201), which is a stretchable and transparent material. The fabrication approach is illustrated in Figure 7. The sensor is U-shaped to increase the length of the conductive path, consequently, achieving higher sensitivity during bending.

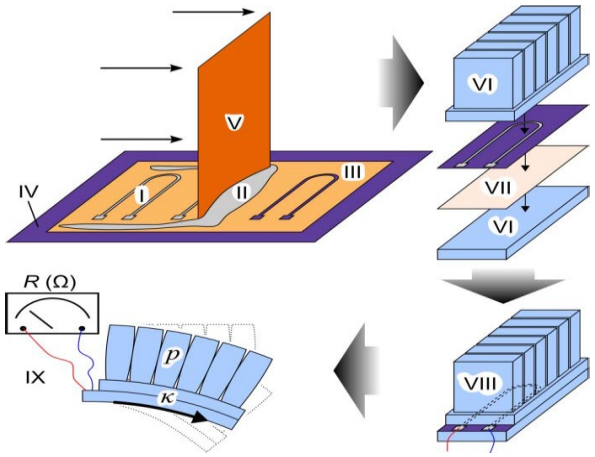

Figure 7. *Schematic for Screen printing U-shape resistive type sensor and integration into soft actuator* [10]

The results showed a linear relationship between the curvature of the sensor and the electrical resistance measured across the pads of the sensor. However, they found that the sensor has a maximum hysteresis of 17%.

From the perspective of flexibility, this type of sensors can be used for bending estimation, but it cannot be used for estimating the applied force.

Correspondingly, the piezoresistive sensor shows response to the external stimuli by interpreting it to variation in electrical resistance, however, the technology of piezoresistive sensor differs from its counterpart in the resistive type sensor. In piezoresistive type, the mechanism leading to the phenomenon of piezoresistivity can be elaborated by quantum tunneling conduction [35], which occurs in the case of conductive composites. Quantum tunneling phenomenon happens when the conductive particles being extremely close to each other to the level that allows the kinetic energy of localized electrons to be higher than the potential energy superimposed by barriers between these particles. Typically, the composite consists of two materials: First, the substrate that represents nonconductive polymer with an elastomeric property. Second, the active material, which is conductive filler encapsulated inside the elastomer. Primarily, the barrier

between conductive fillers impedes the flow of electrons by raising up the energy bandgap of the composite. After deformation, the fillers come close to each other allowing reduction in tunneling barrier for electrons, which lead to a reduction in energy bandgap, and accordingly, decreasing the electrical resistance of the material.

Kim *et al*. [36] discussed the result for measurements conducted on carbon nanotube (CNT)/polydimethylsiloxane (PDMS) composite-based sensor. They showed the steps to fabricate CNT/PDMS composite. It is found that the conductivity of the composite depends on the concentration range of CNT inside the composite. In the light of what mentioned previously, CNT is the conductive filler and PDMS is the elastomer.

Nevertheless, the weight volume of CNTs is crucial to control the properties of the material; consequently, another important parameter should be defined to ensure the piezoresistive property of the composite. This parameter called the percolation threshold (Figure 8). It is the threshold, whereas, increasing the concentration of CNTs beyond it, lead to converting the composite into a conductive material. The reason behind this phenomenon that after bypassing the threshold, fillers come to contact with each other and forming conductive paths inside the composite[35].

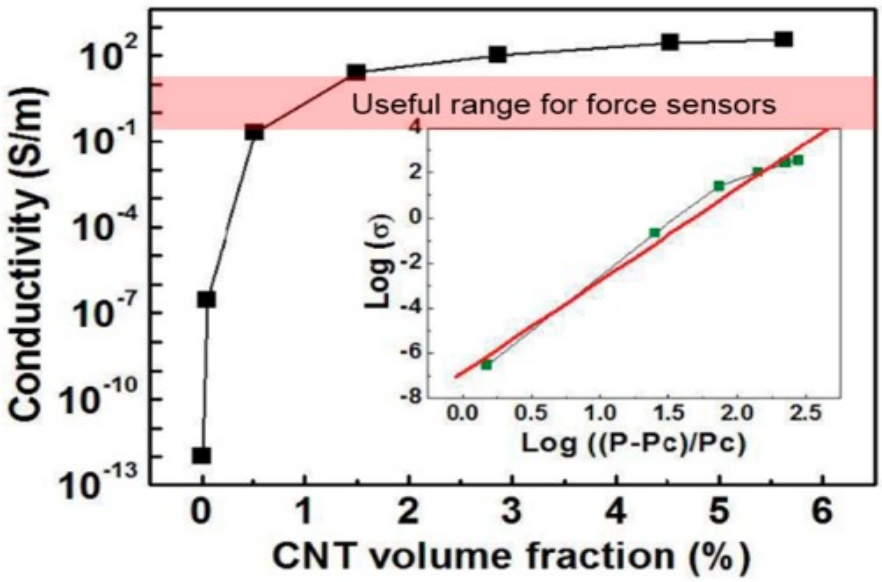

Figure 8. *The variation of electrical conductivity in response to variation of CNT concentration with emphasize on the percolation threshold* [37]

From Kim *et al*. [36] experiment, it is found that 1% of MWCNTs from the total weight volume of the composite is a good range to work in the piezoresistive region.

Overall, it is found that flexible piezoresistive sensor showed high sensitivity and good response to an external stimulus such as force, twisting and bending. The key parameters of the sensor can be highly controlled and improved by determination of the type of elastomer and the external electronics to acquire the signal. The piezoresistive sensor has some commons with the resistive type sensor; one of these commons is instability because of temperature variation; however, it can be compensated by using Wheatstone bridge as we explained in the section of resistive type sensor. Moreover, unwanted phenomenon such as hysteresis can be reduced drastically by using a mathematical model (eg. Duhem model) as it is suggested in [38].

One of the disadvantages of the resistive and piezoresistive sensors are the instability owing to environmental effects such as temperature. Accordingly, configuring the sensor to special circuitry such as the Wheatstone bridge can provide a solution for tackling this drawback [39]. There are different configurations can be considered in the case of Wheatstone bridge such as half-bridge strain gauge circuit or full-bridge strain gauge circuit as it is seen in Figure 9. At balance, the voltmeter reading between the two nodes is equal to zero and circuit derivation ends to this formula

$$\frac{R1}{R3} = \frac{R2}{R4}\,. \tag{3}$$

The configuration should be chosen based on the application requirements. As an example, if the target is to compensate for temperature effect, then a half-bridge circuitry will be enough. To both enhance sensitivity and to compensate for the temperature, full-bridge circuitry will be a better choice.

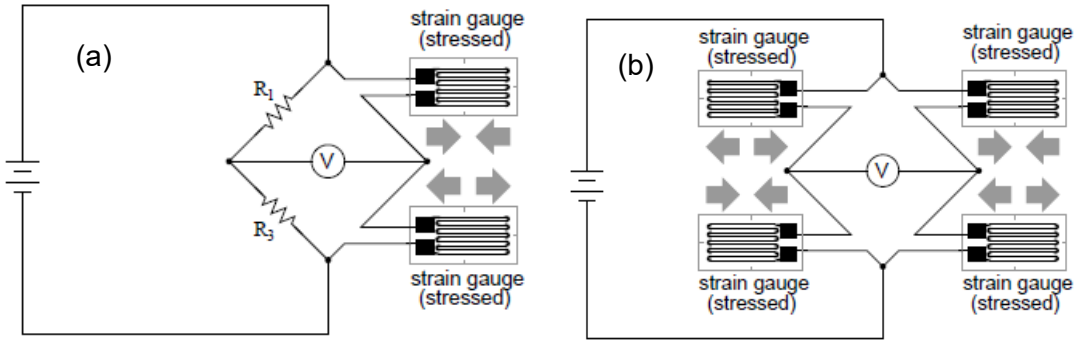

Figure 9. *(a) half-bridge configuration and (b) Full-bridge configuration of Wheatstone bridge* [39]

In conclusion, while the resistive type sensor has the advantage of ease measurement, it has the disadvantage of creep effect, hysteresis and temperature effect [10], [11]. However, it has been reported that such these drawbacks can be mitigated to increase

the accuracy of measurement and in some cases increasing sensitivity by using an electronic circuitry configuration (e.g. Wheatstone bridge).

3.2 Optical type

Principles of operation in optically flexible sensor depends on making use of the optical properties of the material to induce variation in electrical signal when it exposed to physical stimulus. Typically, the device consists of three components: light emitting diode, photodetector and the medium of light transport, which works as a waveguide. The waveguide is designed as a step-index multimode optical fiber. To explain, the optical fiber in this mode composed of two components, the core with a high reflective index and the cladding with the lower refractive index. When a physical stimulus applied on the flexible sensor, the sensor deforms elastically, which cause a loss in the transmitted light across the waveguide due to the properties of the medium represented in the variation in refractive index between core and cladding. This loss in light intensity sensed by PD and converted to variation in the electrical signal [1].

Zhao *et al.* [1] proposed a stretchable sensor, based on optical waveguides, for a soft prosthetic hand. The results were interesting in terms of the performance of the sensor and the compliance with the application. The sensor was able to estimate elongation, bending, and press. The sensor disclosed a high level of precision in terms of signal-to-noise ratio and stretchability.

They used elastomer casting in four steps for sensor fabrication, as shown in Figure 10:

1. 3D printing mold for casting the cladding.
2. Pouring the pre-elastomer in its liquid phase into the mold and demolding it after solidifying.
3. Fill the cladding with the pre-elastomer of the core.
4. Enclose the core by pouring pre-elastomer of cladding.

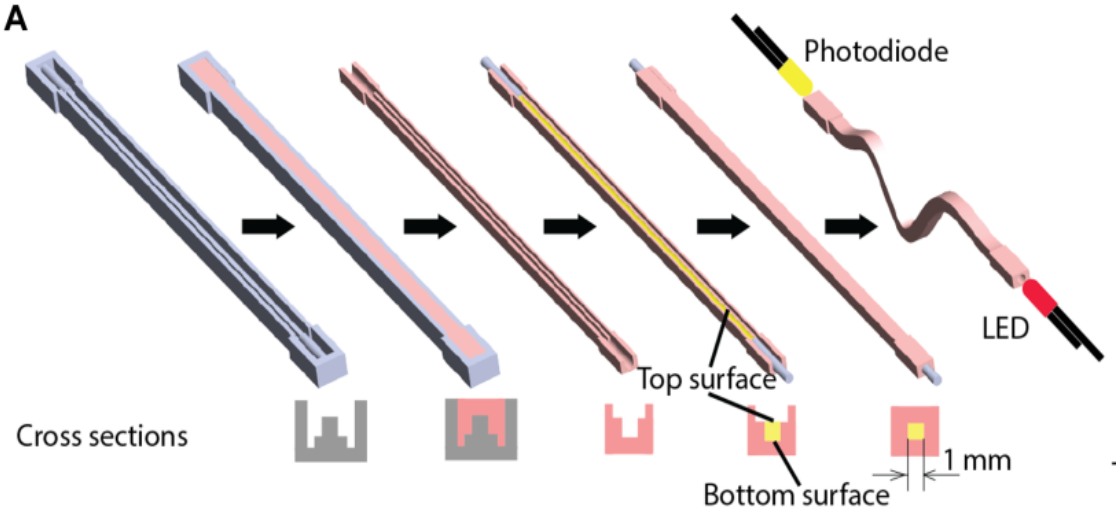

Figure 10. *Elastomer casting steps for optical waveguide fabrication* [1]

Recently, To *et al.* [40] proposed a simpler approach for fabrication of soft optical sensors, which can be integrated into soft robots to provide an estimation for pressure exerted on these robots or strain induced in it due to other mechanical stimuli.

In their proposal, the components of the sensor are similar to the aforementioned sensor suggested by Zhao and his coworkers [1], optical power source to work as a transmitter, light sensor that works as a receiver, and medium represented in a soft optical waveguide that intended for light transmission. However, the difference in this research work that researchers suggested a simpler and straightforward approach for fabrication, as shown in Figure 11. The medium is needed to be elastomeric and transparent; therefore, they used PDMS-based waveguide as a soft-compliant medium for optical transmission. The PDMS is molded as two halves, resulting in a semi-circular hollow channel when the two halves bonded together in a later stage during assembly. The surface of this hollow channel was coated with an inextensible reflective material such as gold. The gold is deposited on the exterior walls of this channel through sputtering deposition in an early stage before halves assembly.

Principles of operation in this device are associated with the loss of optical power, which caused by the microcracks in the reflective surface of the hollow channel. In the intrinsic state of the device, under no external stimuli, the light is propagating normally in the channel from transmitter to receiver. Once mechanical stimuli cause deformation in the inextensible reflective layer, the light starts to escape through microcracks produced in the layer, leading to a loss in power delivered to the receiver.

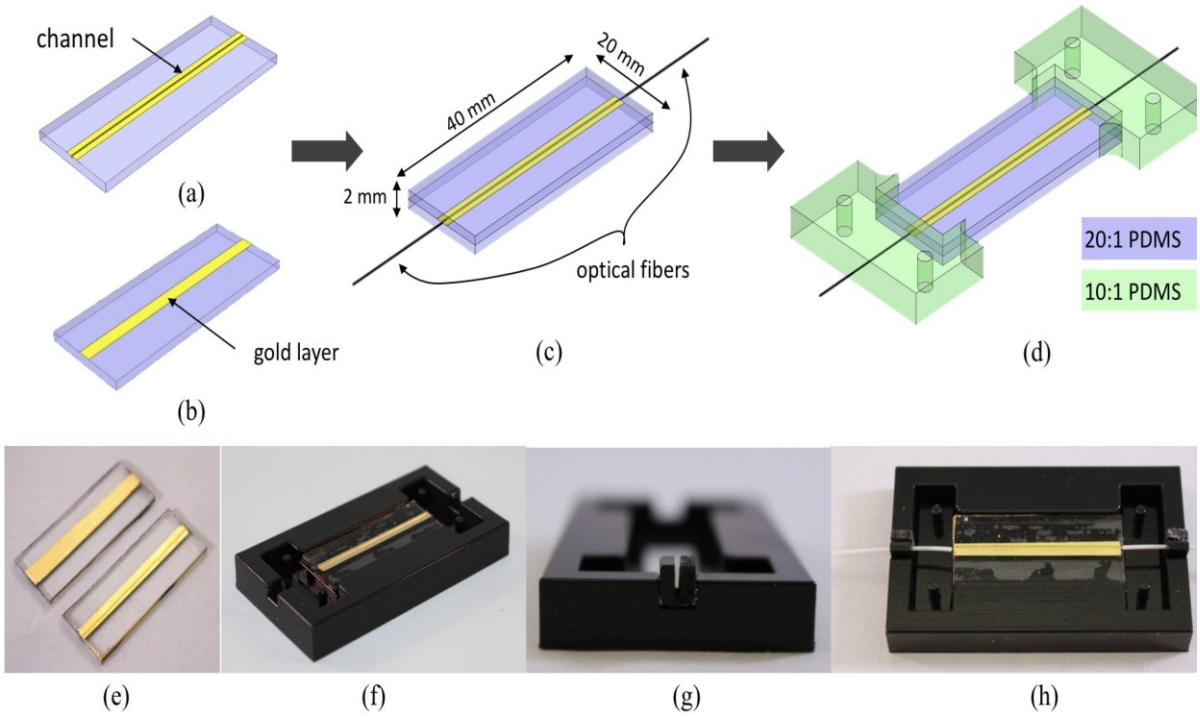

Figure 11. *Schematic for optical sensor fabrication. The sensor is PDMS-based waveguide with a hollow channel coated with gold as a reflective material for light propagation. (a) Upper half with semi-circular channel coated with gold combined to (b) lower half with gold-coated strip to form (c) the assembly with fiber optics connected to endings. (d) Finally, supporting the assembly with the additional structure needed to clamp fibers with sensor body. (e) the two halves after fabrication are inserted in (f) the mold for alignment with the optical fiber. (g) close-up view of the fiber optics slot and (h) the insertion of fiber optics before enforcing the structure with the clamping elastomer* [40]

In conclusion, the optically flexible sensor offers a highly efficient solution for sensory capabilities in the soft prosthesis, especially, when it comes to measuring various types of the physical stimuli such as bending, elongation and pressure. Nevertheless, the implementation needs some level of complexity because it involves the elaboration of multiple components and more fabrication steps to finalize the sensor, in comparison with other simple technologies, such as resistive and piezoresistive type.

3.3 Capacitive type

Electrical capacitance is a phenomenon, which occurs when a dielectric material is sandwiched between two conductive electrodes, which results in the accumulation of electrical charges on the electrodes. This phenomenon is found to be useful in various sensory applications such as humidity, proximity, acceleration, material sorting, liquid level, and pressure.

Principle of operation in capacitive-based pressure sensor depends mainly on the variation in distance between the two electrodes. In general, the value of sensor capacitance is determined by the following equation:

$$C = \varepsilon_r \varepsilon_0 \frac{A}{d} + C_f, \quad (4)$$

Where, ε_r is the relative dielectric constant which filling the space between the two electrodes, ε_0 is the electric permittivity of the vacuum, *A* is the overlapping area between the two conductive plates, d is the separating distance between the two conductive plates and C_f is the constant term which represents the contribution from edges of the electrode, as the edges tend to store more charges than the rest of the electrode. Typically, *A* >> *d*, therefore C_f is a negligible term.

The compressibility range of these sensors, as well as, the electrical properties of the electrodes as a conductive material and the intermediate layer as a dielectric material, affect the sensitivity of flexible capacitive-based sensors, as shown in Figure 12.

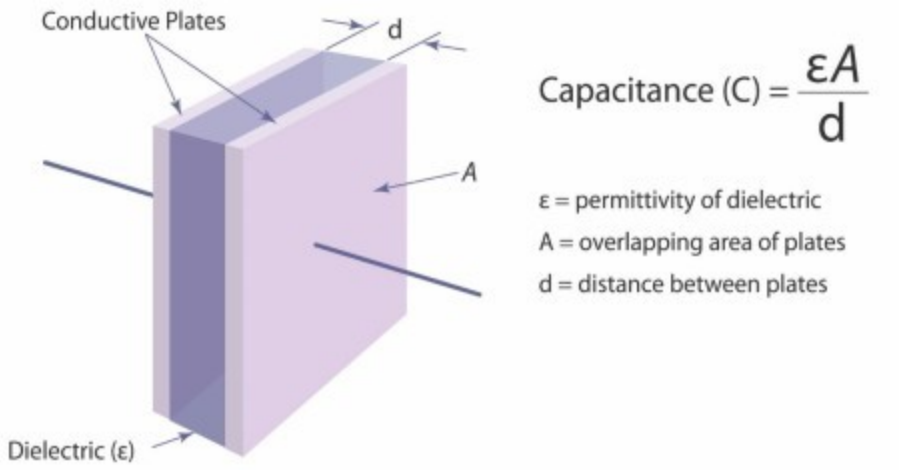

Figure 12. *Parameters to define the capacitive sensor* [41]

Many researchers reported different structures and techniques to enhance the key parameters for these sensors. The sensor sensitivity is affected by the type of dielectric material, such as polyvinylidene fluoride (PVDF) [42], polyvinylpyrrolidone [43] or polysiloxane elastomers[44]–[46]. The sensor structure also affects the sensitivity. As an example, Kang *et al*. [12] suggested using a porous dielectric layer from PDMS. The results were interesting in terms of high stability with multiple operational cycles, high sensitivity, fast response and relaxation time.

Mannsfeld *et al*. [44] demonstrated using photolithography and chemical etching technique for the fabrication of a micro-structured array of PDMS as a dielectric layer; empirically, they compared dielectric layers with arrays of pyramid-shaped structures to dielectric layers with line structures and non-structured dielectric layers. Despite the interesting results related to pyramid micro-structured array, the fabrication technique represented in using photolithography is complex, not vastly affordable and not paving the way for high scale production. One of the advantages of the pyramid micro-structured dielectric layer is that it offers a dielectric structure with a regular morphology, which may be important in some applications that require an equally distributed sensitivity for the spatial pressure.

Recently, Qiu *et al*. [46] suggested a simple, cheap and environmental friendly technique for structuring the dielectric layer of capacitive e-skin, whereas they bio-mimicked the pattern of Calathea zebrine leaf by using it as a replica mold for low-cost micro-structured ionic gel (MIG). The LOD was as low as 0.1 Pa, which is very low compared to a more typical 2.42 Pa [12]. Furthermore, the sensitivity of the sensor was high under conditions of low applied pressure. According to Qiu *et al*. [46], the high-performance renders to the formation of ionic-capacitive interfaces, which stimulate higher change in capacitance more than its counterpart in normal capacitive sensor does. Nevertheless, the proposed design for the e-skin superimposes irregular morphology for the MIG, which shortens the applicability of utilization in specific domains that require distributed sensitivity for the spatial pressure. Moreover, the proposed solution did not offer a solution for robust design in terms of the strong bonding between electrodes and the dielectric layer because the scotch tape was used to align layers of the sensor together.

From the perspective of robustness, in the previously mentioned trials, researchers used Polyethylene terephthalate (PET) or polyimide as a substrate for conductive electrodes. As an example, utilizing ITO-coated PET substrate as in [44] or spraying Silver NanoWires onto a colorless polyimide substrate as in [46]. In both cases, the sensor must be packaged in a specific manner or layers should by laminated by an external substance, which influences the overall performance or the flexibility of the sensor. For instance, Qiu and his co-workers [46] reported using a 3M Scotch tape to bond edges of the device, which superimpose extra-dimensionality and non-efficient solution in terms of uncertainty about layers immobility. Accordingly, all previously mentioned solutions make the sensor efficiency degraded under exposure to special conditions; As an example, using a scotch tape for bonding do not guarantee the preservation of the sensor functionality in the wet environments because the sticky substance in the scotch tape may decompose under the effect of water or other types of liquid.

To summarize, there are many examples of flexible capacitive sensors. Some researchers have fabricated highly sensitive sensors with regular morphology and achieved a unified spatial sensitivity; however, it came on the cost of simplicity and fabrication costs [44]. While, others succeeded to produce a sensor fulfilling many aspects such as simplicity, biocompatibility, and low costs; however, it could not ensure unified spatial sensitivity because of irregular morphology of the dielectric layer of the sensor [46]. None of the previously mentioned solutions offered a solution with fulfilling the combination of these attributes: regular morphology for equally distributed sensitivity, low-cost production, biocompatibility, simplicity, and large-scale production attainability.

As a result, using a 3D printer to fabricate a replica mold to get a structured dielectric layer seems to be a reasonable approach to fulfill the attributes. Structuring by 3D printed replica mold is still more expensive than using natural leafs as replica mold [46], however, it is still biocompatible, lead to conformal structure production, cheaper and simpler than utilization of photolithography for replica mold fabrication [44].

3.4 Comparison of presented sensor technologies

Analyzing the pros and cons of different types of sensors can eventually help to select the most feasible and convenient sensor type for our intended purpose. Based on literature from [3], [11], Table 1 compares the advantages and disadvantages of sensor technologies that commonly utilized in soft robotic applications. Nevertheless, it is important to notice that the comparison is conducted based on flexible type sensors, where the corresponding properties differ from its counterparts in rigid type sensors.

Table 1. *Merits and demerits of the different sensor technologies*

Technology	Merits	Demerits
Resistive	• high sensitivity • low cost • simple fabrication and configuration • utilizable for the measurement of bending or twisting	• low SNR ratio • not suitable for force contact force measurement • hysteresis

Optical	• responsive to multiple forms of deformation • adequacy for force contact measurement • high precision • high signal-to-noise ratio • immunity to electromagnetic interference	• complex approach for fabrication • complex electronics • bulky structure, which, mean that miniaturization is difficult
Piezoresistive	• high sensitivity • low cost • low noise • simple fabrication and configuration • adequacy for force contact measurement	• non-linear response • signal drift • hysteresis, however, it can be compensated by the implementation of the mathematical model [36]
Capacitive	• high sensitivity • low cost • robust • high immunity to noise • simple fabrication • high stability under multiple operational cycles • adequacy for force contact measurement	• longer relaxation time in comparison with previously mentioned technologies due to viscos-elastic properties of the dielectric layer • complex electronics • linearity is dependent on multiple factors, such as sensor structure, electrode material, and dielectric material

Consequently, after considering the simplicity of integration, compatibility with the targeted application and low cost of fabrication, we decided to fabricate capacitive or piezoresistive sensors for our proposed artificial skin and compare their performance. In the following sections, we will explain in detail how these sensors were fabricated and how their performance was characterized. Through the comparative study, minor differences in all key-parameters should be noticed, while, the major difference should be identified regarding the complexity of the needed electronics to interface with the sensor to process the sensor signals.

3.5 Noise

Electrical noise is any undesirable disturbances, which might interfere with the measured signal. We will notice the effect of noise on the measured signals from the fabricated sensor, as we will see in chapter 7; therefore, we need first to understand the meaning of the electrical noise. Moreover, identify sources of electrical noise, available solutions to tackle it and finally how to apply the solution on our application

Origins of the noise can be rendered to external or internal sources. The external sources can be magnetic, electric or cross talk, which simply represent a parasitic capacitance generated when two cables or more be so close to each other; however, electromagnetic source still be the most popular one among the external sources for noise because it originates from current passing in the cables, where, every wire acts as an antenna. Regarding the noise of the internal sources, there are multiple sources for it such as Shot noise, thermal noise, flicker noise, burst noise and avalanche noise [47].

Shot noise is analogs to the current flow in conductor or semiconductor; for further explanation, it originates from the random fluctuations of the charge carriers in the conductive medium, which typically caused by the potential barriers in the conductor because of the existence of some impurities in the medium. Thermal noise is originating from the thermal stimulation of electrons in the conductor, whereas, heat disturbs the normal motion of electrons induced the difference in potential across the conductor. Flicker noise that known as 1/f noise is analogs to imperfections in the crystallinity structure of the semiconductor device; therefore, it exists in all active devices and varies inversely with the switching frequency in the direct current-based devices. Burst noise is analogs to the discrete high-frequency pulses, however, the control over it is difficult to be realizable. Avalanche noise is associated with PN-junctions when it operates in the reverse direction mode; as an illustration, the junction under the effect of reversed electric field has a higher depletion region, which excites the electrons with high kinetic energy to collide with atoms of the crystal and generate additional electron-hole pairs. Consequently, generating random current pulses, which are noisier in comparison with its counterpart in shot noise [47].

To mitigate the magnitude of noise, there are some precautions can be considered to limit the effect of external noise such as shielding of noise sources and noise-vulnerable components, avoiding ground loops that facilitate noise propagation, and

positioning the system components properly by assuring enough segregations between system assets to avoid cross-talk [48]. Nevertheless, noise based on internal sources will remain a problem, which can be tackled by filters.

Filters can be classified as analog filters or digital filters. Analog filter is an operational amplifier-based electronic circuit, such as the one shown in Figure 13; it works with continues signals. Conversely, the digital filter is a set of algorithms applied to the processing unit and deals with the signal only after discretization in digital format. Despite, both types can apply most functionalities, the analog filter is superior in terms of the amplitude dynamic range and the frequency dynamic range, however, it needs integration of electronic components to fulfill the target and it will never be as accurate as a digital filter. The components of the analog filter have some level of tolerance for variation, which will be reflected on the overall performance by some residual ripples in the pass-band of the filter under step input response. On the other hand, the digital filter is superior in performance and possesses a higher potential for implementation because of the easiness associated with tuning the parameters to meet the requirements. Moreover, the digital filter is better than the analog filter when considering other characteristics such as stop-band attenuation and roll-off. [49].

Filters have many designs such as low-pass filter, high-pass filter, Band-pass filter, and many others, whereas, each design is meant to allow the passing of specific band of frequencies and blocking frequencies outside this band.

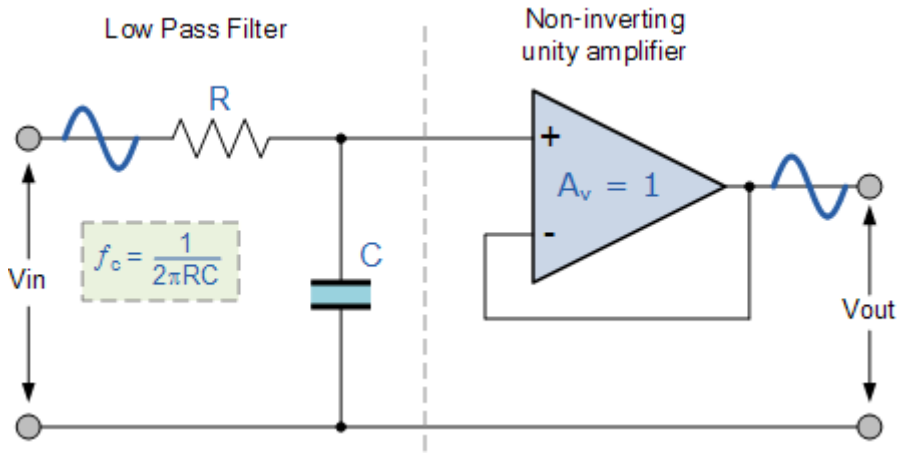

Figure 13. *Schematic of the non-inverting low-pass filter* [50]

Considering a capacitive sensor as a case study to observe the applicability of noise filter integration with the sensor, we can see that low-pass digital filter will be an appropriate choice for integration with the capacitive sensor if we are aiming for noise

elimination and highly efficient readings from the sensor. The variation in capacitance must be represented in another processable variable such as voltage or frequency. Accordingly, the sensor needs to be interfaced with readout circuitry, which will discretize the continuously acquired signal from the sensor such as in the case of using an Integrated circuit (IC) of AD7147 [47], as shown in the datasheet of the chip. The IC is sampling the signal at a specific rate defined by the chip programmer. Furthermore, it has a built-in algorithm to track the signal levels, whereas, it can adjust the threshold continuously in synchronization with the change in the ambient level. We can clearly see that with such this approach of digital abstraction [51], which mean discretizing the signal to high and low level relative to some referenced value (Figure 14) and with the ability of IC chip to define a threshold for distinguishing the signal from noise, the associated noise with the capacitance signal readings will be filtered automatically. This showcase demonstrates how much is beneficial using the IC chip for processing the signal acquired from the capacitive sensor.

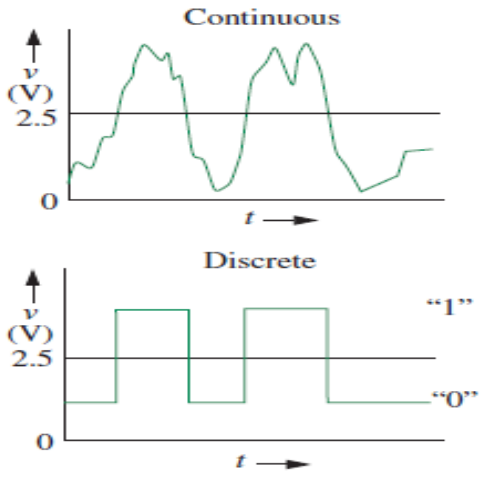

Figure 14. *Signal discretization at voltage reference of 2.5 V* [51]

4. FABRICATION METHODS FOR ARTIFICIAL SKELETON AND SKIN

As we mentioned in Chapter 2 that tendon-driven SRH manifests as a suitable option for reasons of simplicity, durability, and compliance with sensor integration. The following sections will detail the performed steps to fabricate both the artificial skeleton and the artificial skin.

4.1 Design and fabrication of artificial skeleton

Chapter 2 introduced the design concepts for the anthropomorphic robot hand and how it can be actuated. Correspondingly, as we are aiming for applications in bionics and industrial applications to maneuver loads dexterously, the tendon-driven mechanism offers a good approach in terms of simplicity and compliance with the targeted application. To explain the mechanical design of the hand, each finger of the hand is composed of three subcomponents, as seen in Figure 15. The components are printed separately and later assembled together. Each component of the finger has a spherical tip in one end (bin) and a spherical cavity in the other end (ball), where, these features facilitate the assembly and disassembly of the components by gently pressing it toward each other to form the final articulated structure of the finger (Figure 15d). All components were designed using Solidworks® CAD software. [26]

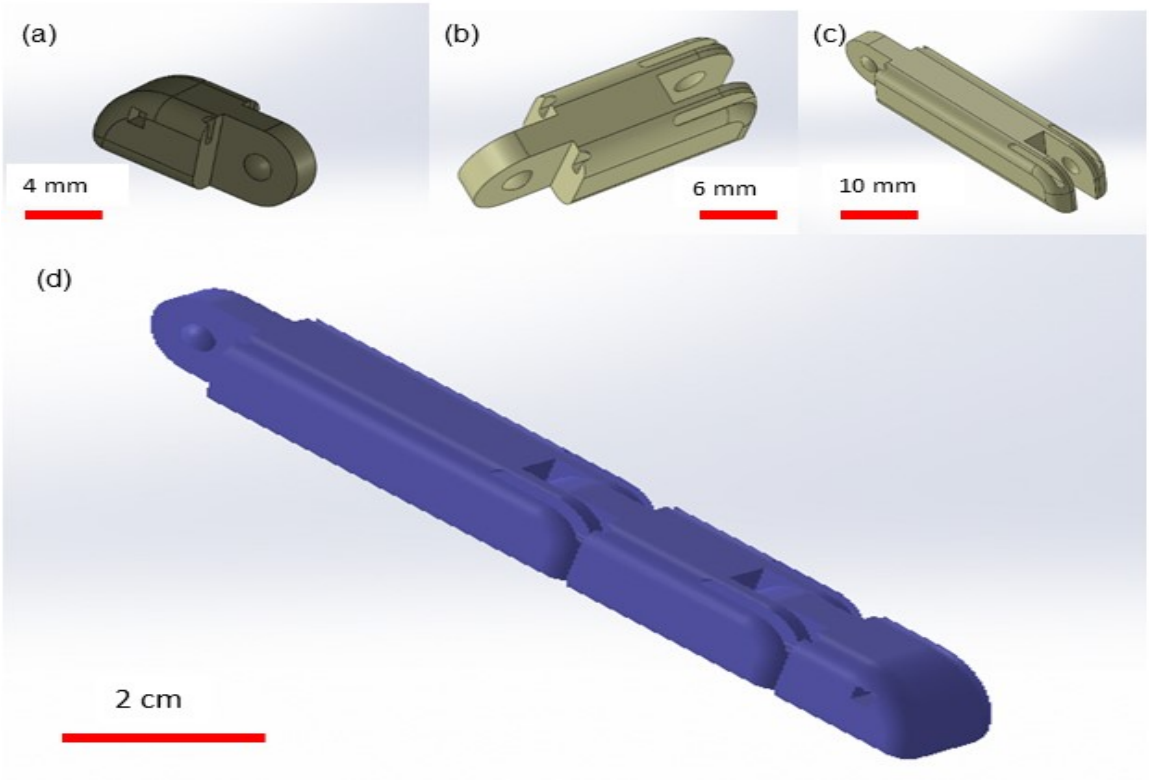

Figure 15. *The three components of the finger before and after assembly, a) the fingertip, b) intermediate phalanges, c) Metacarpals, and d) articulated structure of the robotic finger after components assembly*

Once the design was finished, it was converted to STL file format, which is readable by 3D printers. FDM printer (Prusa i3 MK3, CZECH REPUBLIC**)** is used to print all components of the artificial skeleton. Polylactic acid (PLA) is used as a filament for components printing owing to its features represented in, low cost, and abundance [52], which made it a sufficient selection for our application.

The palm of the hand was designed and printed similarly as the fingers, however, the only difference that it is designed as one component with a specific geometry that enhances gripping capability by considering a regularly distributed slots along the curved axis to facilitate fingers connection to the palm, as shown in Figure 16. Channels were embedded inside the palm structure; these channels work as routes for tendons to move freely in two directions and actuate the robotic hand fingers.

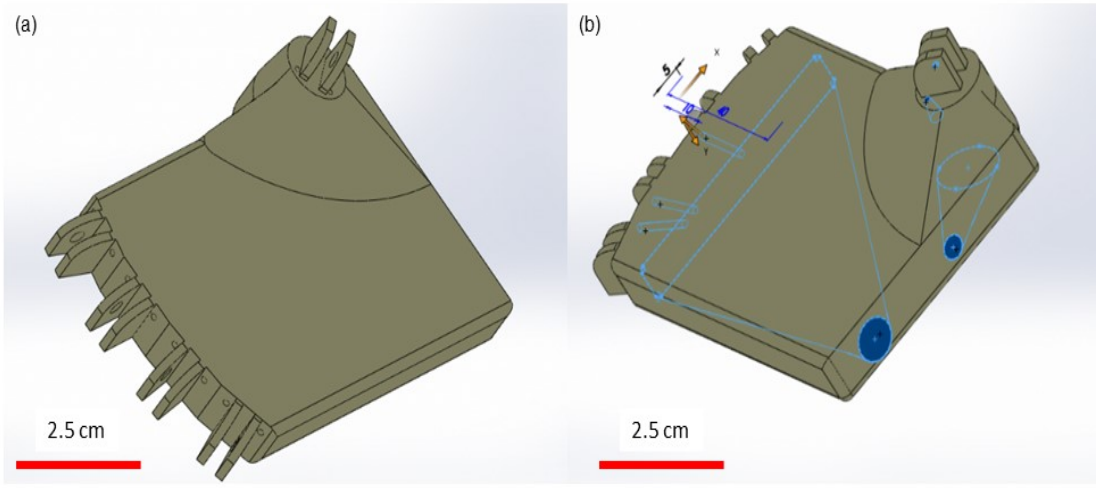

Figure 16. *The palm of Robotic hand with a) normal view, b) view with emphasize on the channels embedded inside the palm to facilitate the tendon-driven mechanism to actuate the fingers*

4.2 Design and fabrication of the artificial skin

The steps to fabricate the artificial skin are shown in Figure 20. In the first step, the mold (Figure 17) for the skin of the palm is 3D printed using a FDM printer (Prusa i3 MK3). The low resolution of the FDM printer was found to be enough for the features in these molds. The mold had three components, which were assembled during the process to form the structure of the artificial skin.

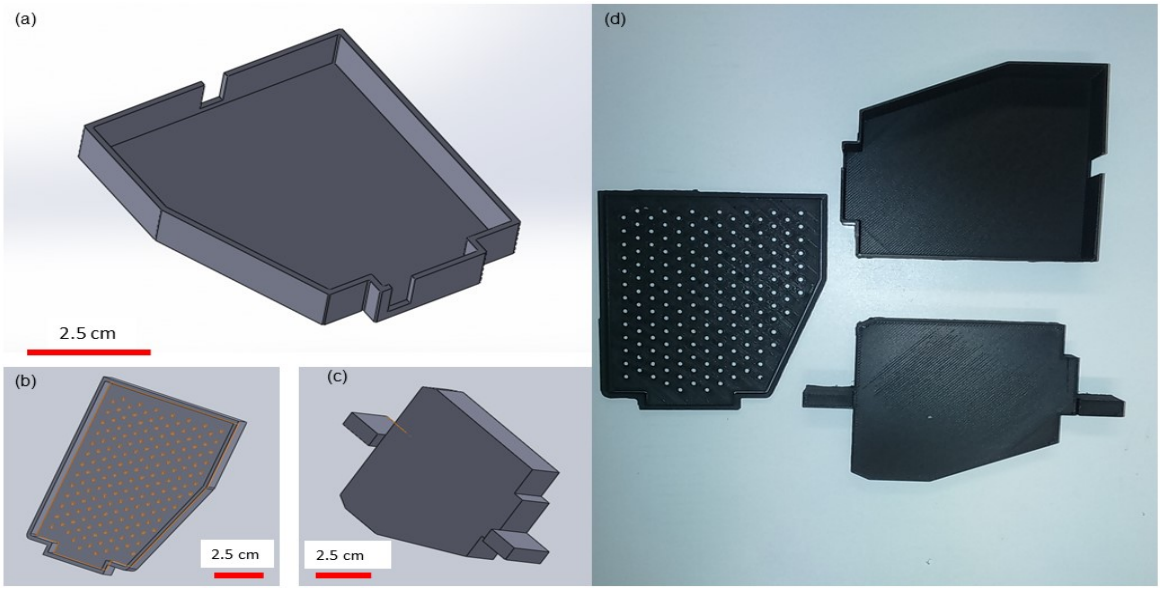

Figure 17. *The three components of the mold for palm artificial skin before assembly. The CAD design of a) Lower component, b) Upper component and c) Core of the mold. d) The 3D printed mold of palm skin*

The mold for casting the skin of the fingers are shown in Figure 18. For these molds, SLA printer (FormLabs, U.S.A [28]) was used to achieve a high-resolution quality. It was crucial to get a high-resolution print for finger mold owing to the tiny features of these components, which was necessary for fitting the components together during assembly.

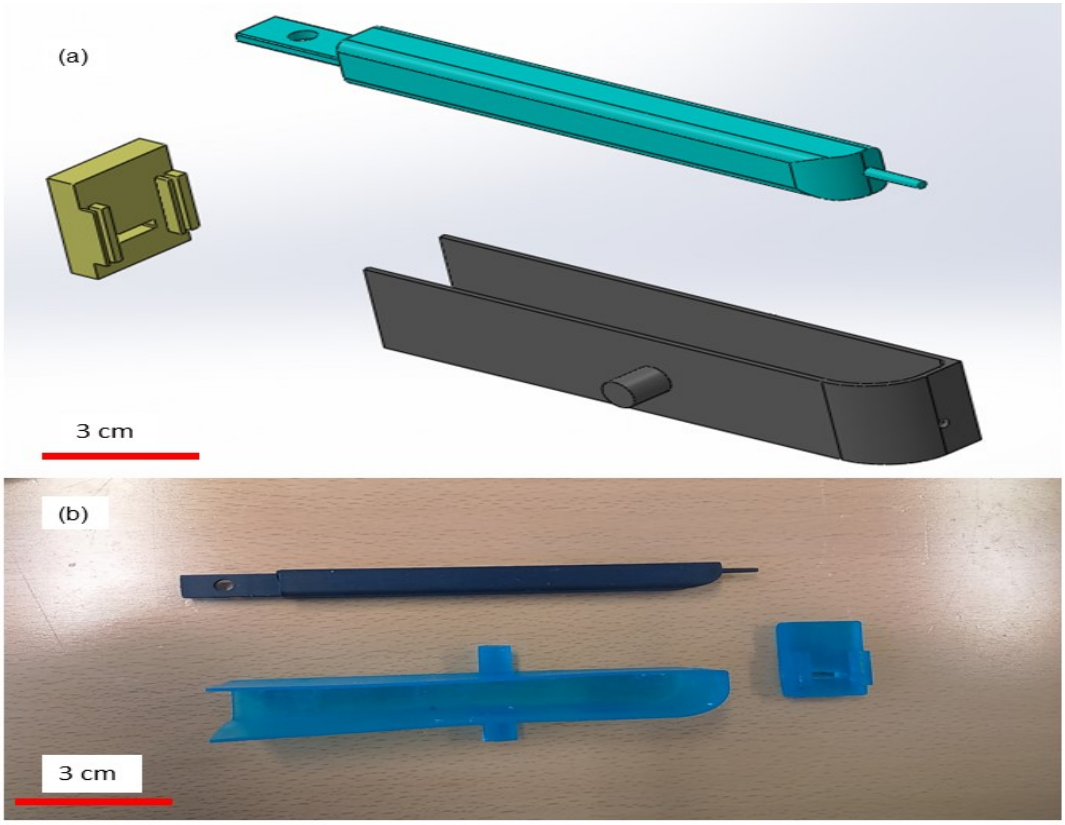

Figure 18. *a) The CAD design of the three components of the mold to fabricate artificial skin of the finger. b) The 3D printed mold of finger skin*

To form the elastomeric skin of the finger, the components are aligned together to form the assembly shown in Figure 19. In this case, it was enough to press the components gently toward each other after alignment to start directly the artificial skin molding process. However, to ensure the robustness of the structure and the prevention of any pre-elastomer leakage during the degassing phase, a hot glue gun is used for bonding the components together.

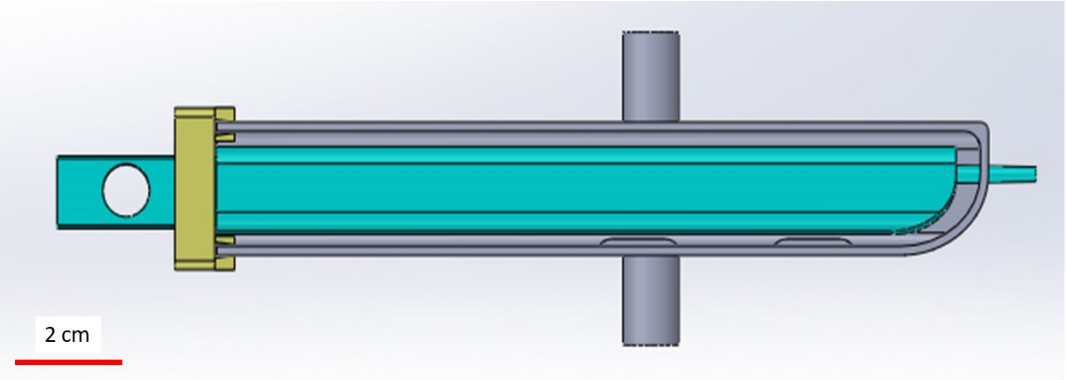

Figure 19. *The mold for artificial skin of the finger after assembly*

The following steps describe the whole implementation of an elastomer casting process to form the artificial skin of the finger (Figure 20):

1. The pre-elastomer is prepared by mixing the two polymers and pouring inside this mold (Figure 20a, 20b and 20c, respectively).

2. Degassing the pre-elastomer for 10 minutes inside the vacuum chamber to ensure the removal of air bubbles from it (Figure 20d). Experimentally, 10 minutes was found to be the optimum time for extracting air bubbles from the pre-elastomer

3. Leaving the pre-elastomer to cure in room temperature to get the artificial skin with elastomeric properties after 24 hours.

4. Demolding the elastomer to use it as artificial skin (Figure 20e) by enfolding the artificial skeleton with it (Figure 20f).

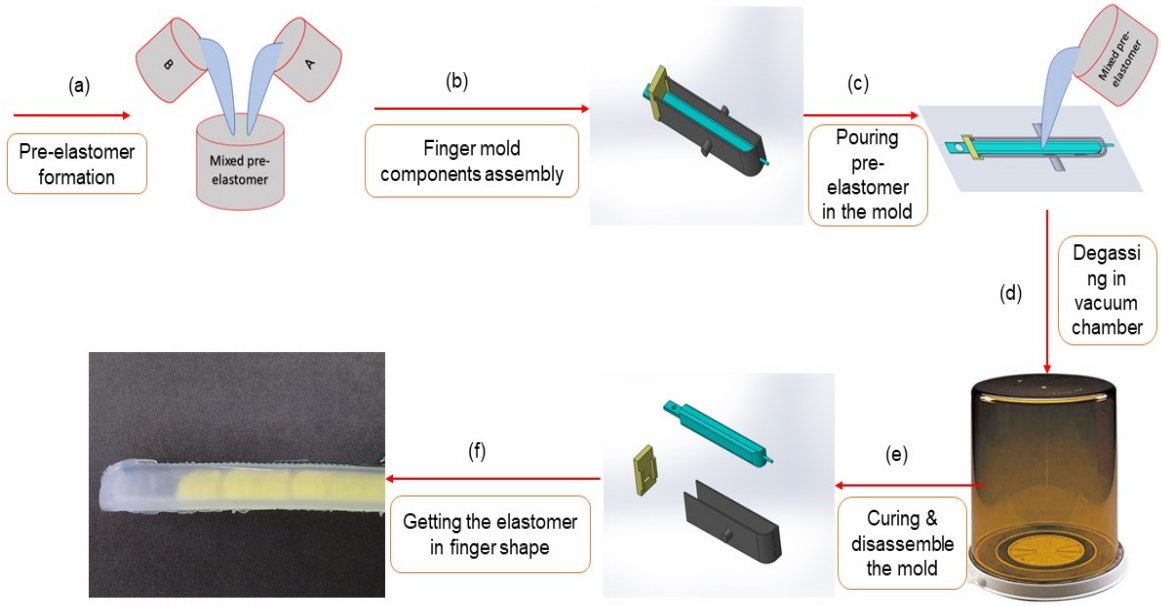

Figure 20. *Schematic description of the process for artificial skin fabrication*

4.3 Materials used to fabricate artificial skin

There are many materials provided by SMOOTH-ON [32], that can be used as an artificial skin for our SRH. To explain, polysiloxane rubber can be categorized according to different parameters, such as mixed viscosity, pot life, demold time, hardness and elongation at break. All or most of these parameters should be considered seriously according to the targeted application and the circumstances of the experiment. As an example, mixed viscosity is an important parameter when using a replica mold with tiny features, where, it is difficult for the viscous polymer to interpose and fill these tiny features; in contrast to low viscous polymer, which can interpose between these features efficiently. Furthermore, pot life is a crucial parameter to ensure the success of the experiment because it gives an indication about the available time between mixing and pre-elastomer transition to elastomeric state and becoming non-soluble. Nevertheless, the most important parameters for the final integration of these materials in a specific application are the softness and the maximum strain, which are explicitly defined by shore harness and elongation-at-break, respectively. After checking the various polysiloxane rubbers offered by the company, the most three compatible materials were selected to be utilized in the different fabrication phases, as we will show in Chapter 5 during the integration of capacitive sensor in the artificial skin. Table 2 lists the different

characteristics of these three materials.

Table 2. *Comparison of the three utilized polysiloxane materials*

Material	Dragon Skin 30	Ecoflex 00-30	Dragon Skin 10
Mixed Viscosity	20 Pas	3 Pas	23 Pas
Pot Life	45 minutes	45 minutes	8 minutes
Cure Time	16 hours	4 hours	75 minutes
Shore A Hard-ness	30	00-30	10
Die B Tear Strength	18.914 kN/m	6.655 kN/m	17.863 kN/m
Tensile Strength	3447.5 kPa	1378.95 kPa	3275.011 kPa
Elongation at-Break	364 %	900 %	1,000 %

These three materials have been tested to find Ecoflex 00-30 is the most suitable choice for artificial skin without any sensation capabilities, because of its low mixed viscosity, comparatively long pot Life, low Shore A hardness and high elongation at break.

5. METHODOLOGY FOR SENSOR FABRICATION AND IMPLEMENTATION

To design tactile pressure sensors for robotic fingers, several aspects need to be considered: type of the signal extracted (e.g. capacitive or resistive), the pressure range of the sensor, the mechanism for extracting this information and characteristics of the robotic finger.

The tactile pressure sensors should enable the SRH to control the grasping force exerted on targeted objects. Because the grasped object might contact any or all of the three phalanges of each finger, we designed every phalange to have one sensor pad, as shown in Figure 21.

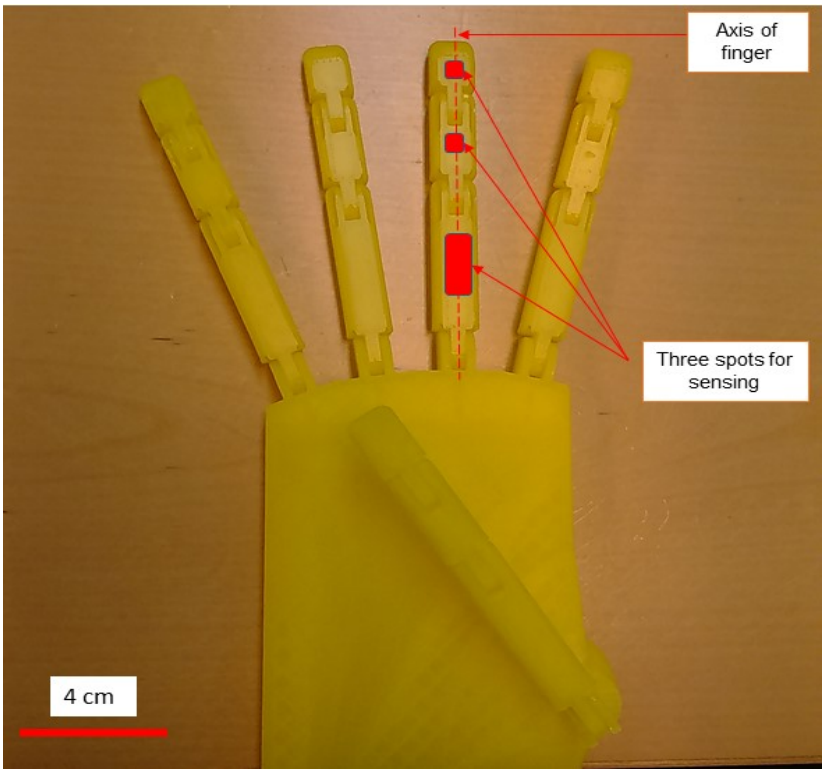

Figure 21. *The printed robotic hand with an illustration of the proposed positions for sensor pads to ensure an inclusive mapping of pressure exerted on the hand*

Within this chapter, we are going to show the steps for sensor fabrication for both piezoresistive and capacitive type, and compare the utilized technologies in the fabrication of both types. Finally, we will show how the sensors were integrated into the artificial skin of the SRH.

5.1 Design and fabrication of piezoresistive type sensor

To make a piezoresistive sensor, we fabricated three layers: upper electrode, a lower electrode, and piezoresistive fabric resting between the two electrodes. PET is used as a substrate for sensor electrodes. A screen printer was used for patterning the conductive electrode on a PET substrate (0.434 mm, Amazon). [10] A screen with patterned mesh (500*300 mm) with the design shown in Figure 22b was ordered from Finnseri Oy (Finland)

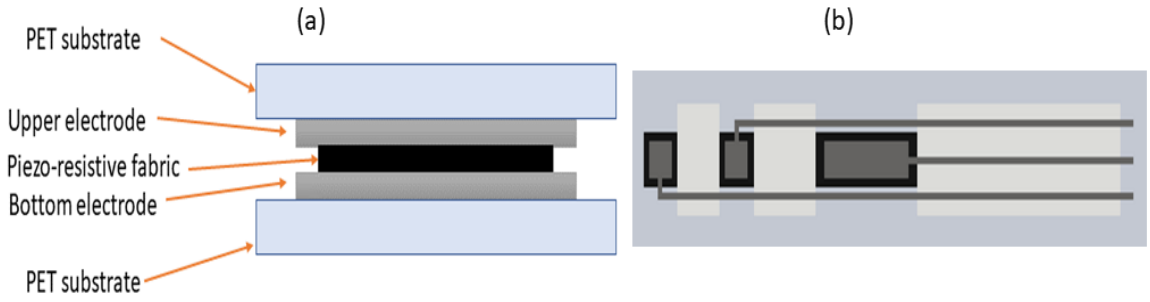

Figure 22. *Schematic description of the sensor design: (a) Side view and (b) top view, where dark silver hashing denotes electrodes, white hashing denotes isolative layer between electrodes, black hashing denotes piezoresistive fabric and light silver hashing denotes the PET substrate*

The fabrication steps for the sensor are:

1. Lay the PET substrate beneath the screen

2. Spread 50 ml of conductive ink on the top of the screen. In this work, we used silver ink (ECM / CI-1036), as it is known by adequacy for applications with stretchable and flexible conductive ink [53].

3. Sweep the ink over the screen by the squeegee, where the ink flow through the patterned mesh on the screen to deposit on the substrate beneath it, duplicating the patterned form of screen mesh.

4. Cure the printed substrate in an oven at 120 °C for 10 min.

5. Laser cutter (epilog laser fusion 75 watts, USA) is used to shape piezoresistive fabric (Eeonyx, USA) into two squares and one rectangular shape to get the three pads as it is seen in Figure 23. The upper and intermediate pads were cut at square shapes (5*5 mm), while, the lower sensor pad is cut at rectangular shape (5*20 mm). The laser cutting parameters are adjusted to use 70% of maximum power, 60% of the maximum speed, 20% of the maximum frequency.

6. Place the fabric pieces and a thin isolative layer between the electrodes. The fabric is fitted between the conductive pads and the isolative layer is placed between the tail of two electrodes to ensure no direct contact between it.

7. Press on the whole structure by passing an iron over it to ensure the adhesion between the top and bottom electrode substrates, which is necessary to encapsulate the sensor and preserve the alignment of the stacked layers.

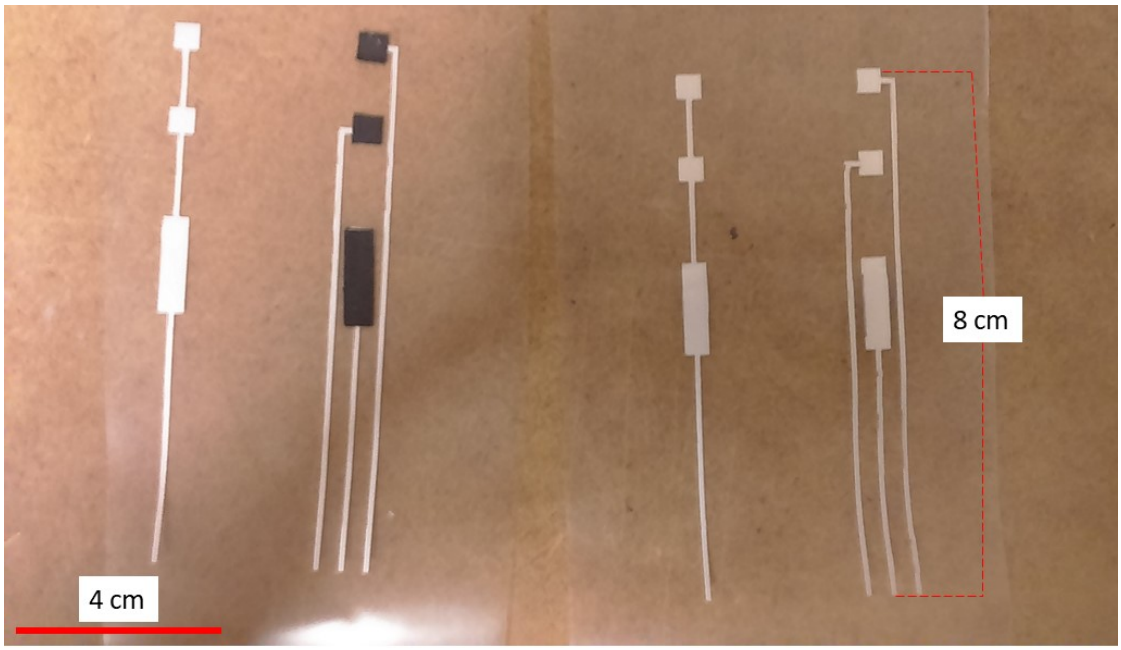

Figure 23. *Captured image of the printed electrodes and the laser-patterned piezoresistive fabric*

Finally, metallic pins (1.27 mm) were fastened to electrodes by using a crimping press (CrimpFlex™, nicomatic, France) to facilitate attaching electrical wires to the electrodes, as seen in Figure 24. Moreover, to ensure complete isolation between the electrodes and avoiding any short circuit between the electrode terminals, heat shrink tubes are used to wrap the exposed metallic pins of the four electrodes.

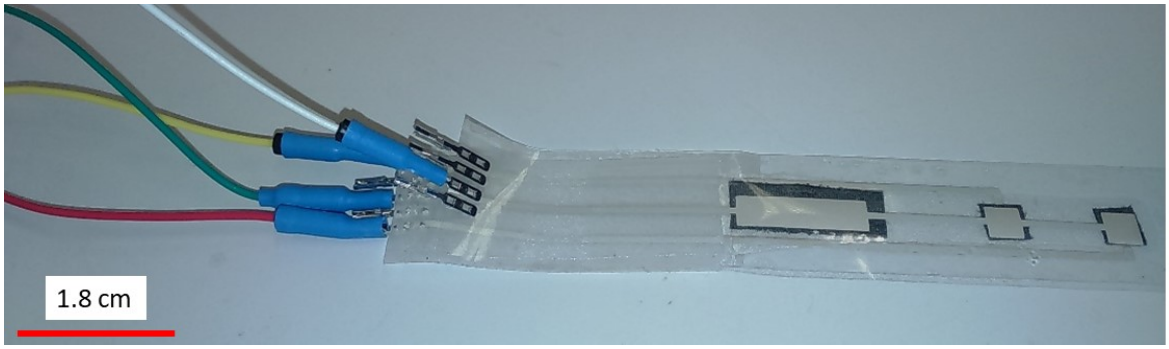

Figure 24. *Image of the piezoresistive sensor in the final form after pins and wires attachment*

5.2 Design and fabrication of capacitive type sensor

To fabricate a flexible capacitive type sensor, we used a conductive fabric (Eeontex) as the electrodes of the sensor. The conductive fabric we used is a normal cotton fabric, produced by the textile industry, but heavily doped with conductive nano-/microwires or nano-/microparticles. [54] The concentration of the conductive filler surpasses the percolation threshold and transfer the composite from insulative to conductive region. The reason for choosing the conductive fabric as the material for electrode fabrication is that it strongly bonds with polysiloxane rubber, by interlocking the elastomer with the fibers of the fabric.

We used the laser cutter (epilog laser fusion 75 watts, USA) to cut the conductive fabric to the shape of the electrodes (The parameters are adjusted as the same one used for aforementioned piezoresistive fabric). The conductive fabric is shaped with the same design used for the piezoresistive fabric; however, the size of electrode pads was a little higher. Where, the upper and intermediate pads were cut at square shapes (10*10 mm), while, the lower sensor pad is cut at rectangular shape (10*17 mm)

We used 3D CAD modeling software Solidworks®, (Figure 25) to design the replica mold and 3D-printed these molds using SLA 3D printer. The microstructured halve of the mold is used for structuring the dielectric layer morphology with a micropyramidal array.

Steps of the capacitive sensor fabrication process are shown in Figure 26. The fabrication process of the lower part of the sensor, which includes the structured dielectric layer bonded to a sheet of conductive fabric, was the following:

1. Mix the two components of Ecoflex 00-30 silicone elastomer by 1:1 ratio in weight to form the pre-elastomer in overall weight equal to 40 gm. Ecoflex 00-30 was used because it has low mixed viscosity, which was supposed to be beneficial for the material to interpose through cavities of the mold

2. Pour the pre-elastomer on the lower mold component

3. Degas the mold with the pre-elastomer for 10 minutes inside a vacuum chamber.

4. Stack a sheet of the conductive fabric on top of the pre-elastomer before it has cured.

5. Press the fabric in direction of the perpendicular axis of the mold by sandwiching the fabric between the upper mold component and lower mold component. It is an important step because it ensures minimizing the offset between the

conductive fabric and the surface of the lower mold. Accordingly, we can acquire a relatively higher value for initial capacitance for the sensor, which is considered as an important key-parameter in the evaluation of the overall performance of the sensor.

6. Cure the whole assembly for 15 minutes in an oven at 70 °C.

7. Carefully remove the assembly from the mold.

The fabrication process of the upper part of the sensor was the following:

1. Mix Ecoflex 00-30 by 1:1 ratio in weight with an overall weight of 10 g.

2. Spin coat the pre-elastomer on a PET substrate. Spin coater speed is adjusted for 800 Revolution per minutes (800 RPM) and kept running for 80 seconds.

3. Place the upper fabric electrodes on top of the coated PET(0.434 mm, Amazon).

4. Cure in 70 °C oven for 15 minutes.

5. Strip the fabric out of PET substrate.

6. Flip out the fabric and put it on PET substrate, where it will be fixed to the substrate by using double-sided sticky tape.

7. Spin coat a layer of pre-elastomer on top of the previous assembly. Unlike the parameters in step 2, spin coater in this step is adjusted for higher speed because less thickness of elastomer was needed in this step. Speed is adjusted for 1300 RPM and held running for 90 seconds.

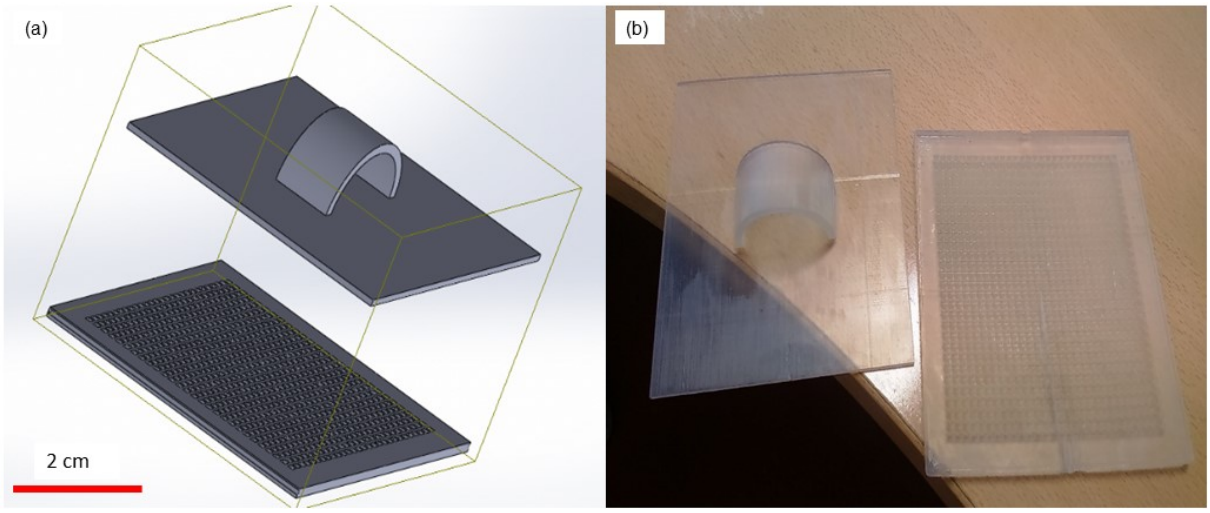

Figure 25. *3D design of mold components to fabricate the upper electrode with the structured dielectric layer. a) The mold design at CAD software, b) The Mold after 3D printing*

The last spin-coated layer on the upper part is used to bond the upper part and the lower part together. To complete the sensor, stack the upper part with the uncured elastomer

on the structured face of the lower part, and cure this assembly in the oven for 10 minutes at 70 °C. Metallic pins for the electric connections were clamped to the conductive fabric to finalize the sensor.

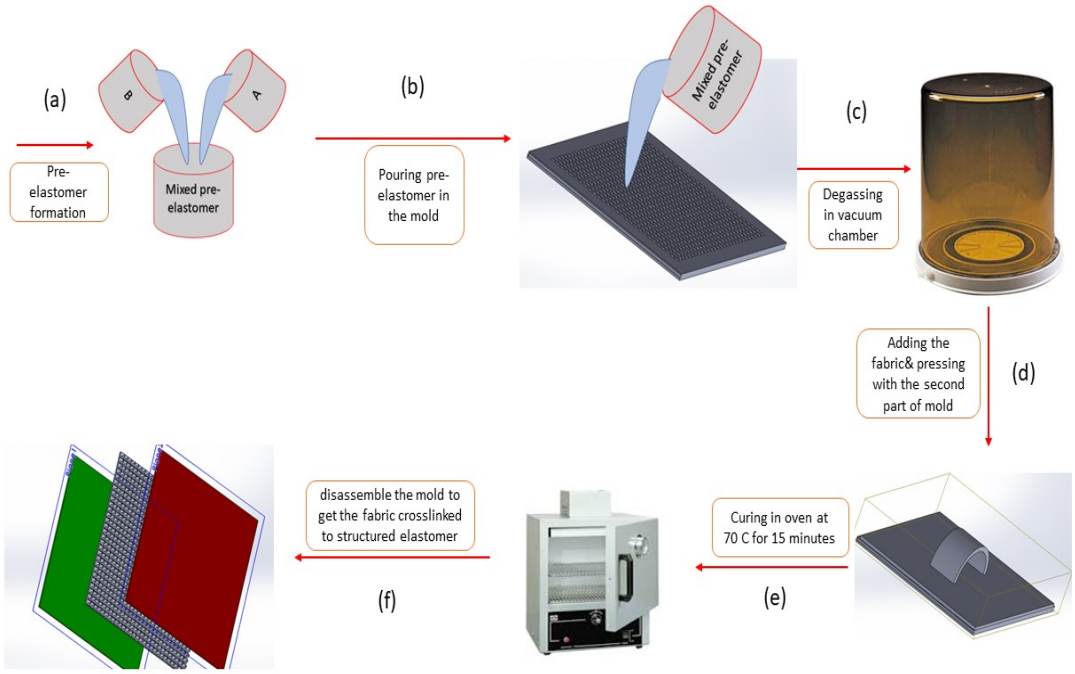

Figure 26. *Schematic description for the fabrication of the upper part of the capacitive sensor*

5.3 Summary of the fabrication processes and materials

The fabrication process and the materials used of the capacitive and piezoresistive sensors fabricated in this thesis work are summarized in Table 3.

Table 3. *Fabrication processes and materials of the capacitive and the piezoresistive sensors*

Sensor type	Capacitive	Piezoresistive
Fabrication tools	• Laser cutter for patterning electrodes • Spin coater for isolative layer application • 3D printer for mold fabrication	• Screen printer for patterning electrodes • Laster cutter for patterning the piezoresistive fabric • Smoothing iron for layers bonding
Materials utilized in the fabrication	• Conductive fabric • polysiloxane Rubber (material with high elastic modulus)	• Conductive ink (ECM / CI-1036) is applicable to be printed on a

	• Metallic pins • The resin is utilized in SLA 3D printer or filament if FDM 3D printer	flexible and stretchable sub-strate • PET substrate • Piezoresistive fabric • Metallic pins
Electrical signal	• Capacitance	• Resistance

5.4 Sensor integration to the artificial skin

The piezoresistive and capacitive type sensors were integrated into the artificial skin in different approaches. The piezoresistive sensor was inserted between the skeleton of the robotic hand finger and the artificial skin, as illustrated in Figure 27. This approach will maximize the protection of the sensor by encapsulating it inside the skin and will also preserve the needed characteristics of a soft touch by making direct contact between the targeted object and the skin. This configuration will likely impose some bias in the initial resistance of the sensor, because of the little stress exerted on the sensor by the artificial skin. However, it will not be an obstacle for measuring any further pressure exerted by external stimuli.

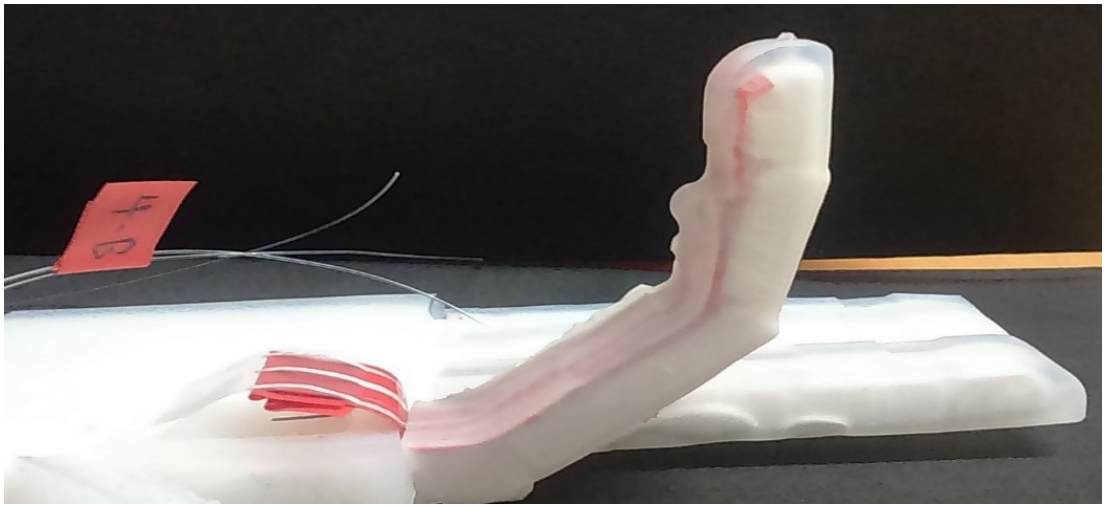

Figure 27. *Piezoresistive sensor inserted between the skin and the skeleton*

The capacitive sensors were integrated directly as a part of the artificial skin, therefore, part of the artificial skin formed the dielectric layer of the capacitive sensor. One set of electrodes was outside the skin, while the second set of electrodes was inside the skin. Consequently, we needed to design a new mold of artificial skin to satisfy the required criteria for sensor integration. As shown in Figure 28; one component of the mold is designed with structured side-wall. The structure is an array of pyramidal cavities, which allow the pre-elastomer to interpose through these cavities and fill it up to get a structured side of the artificial skin.

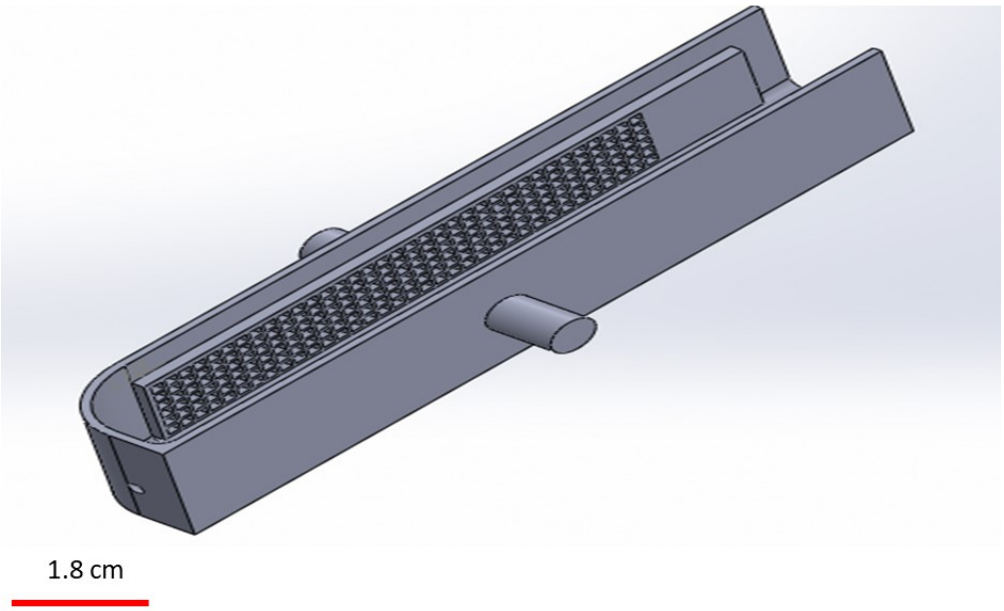

Figure 28. *Sub-component of the mold for finger skin, with an array of pyramidal cavities in one side*

Figure 29 shows schematically the integration of the capacitive sensors into the skin. There is no substantial difference between this process and the normal fabrication process of the artificial skin (mentioned in section 4.2). The only additional step is to include the patterned electrode of conductive fabric during elastomer molding process (Figure 30a), by fixing the three inner electrodes on a sub-component of the mold before the elastomer casting. Dragon Skin 30 was used as the elastomer because it demolded better than the two other elastomers tested (Table 2). The other elastomers suffered from some deformations in the structured side of the elastomer during the demolding process.

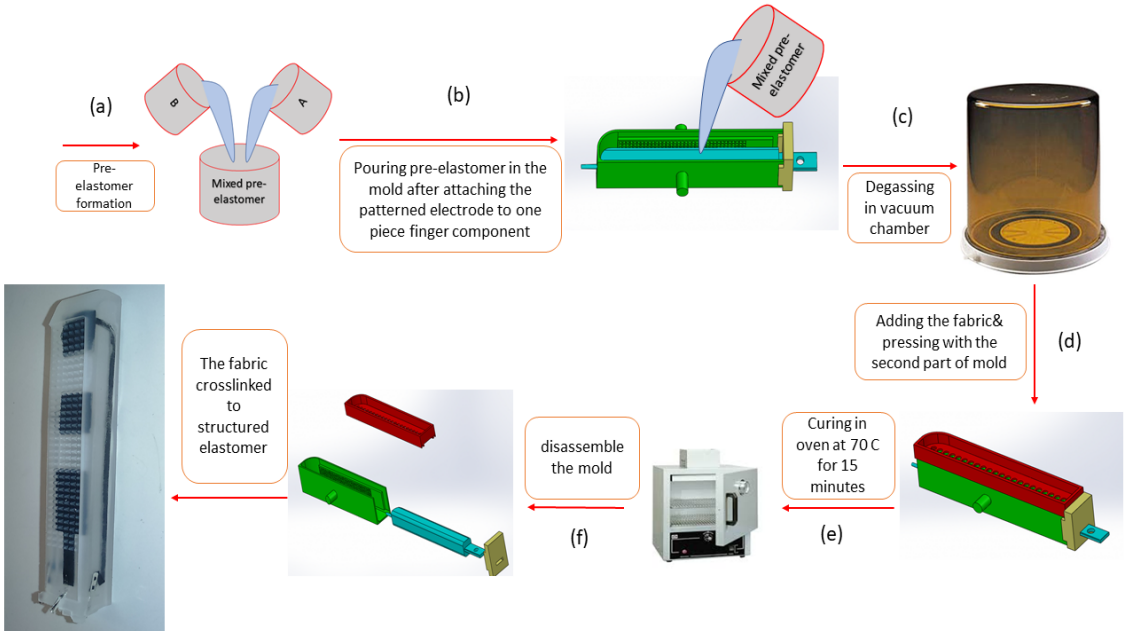

Figure 29. *Schematic description of the e-skin fabrication process*

By completing the process in Figure 29, we get the finger skin with the three-pads electrode embedded directly in it. The skin is strongly bonded to the fabric electrode. To complete the structure, the upper electrode was patterned by laser cutter (Figure 30b). Laser cutter parameters are optimized at 70% of maximum power, 70% of the maximum speed and 20% of the maximum frequency. The upper electrode was positioned on the top of the pyramidal-structured side of the skin, by carefully aligning the top and bottom electrode pads to ensure the maximum overlapping area between the pads.

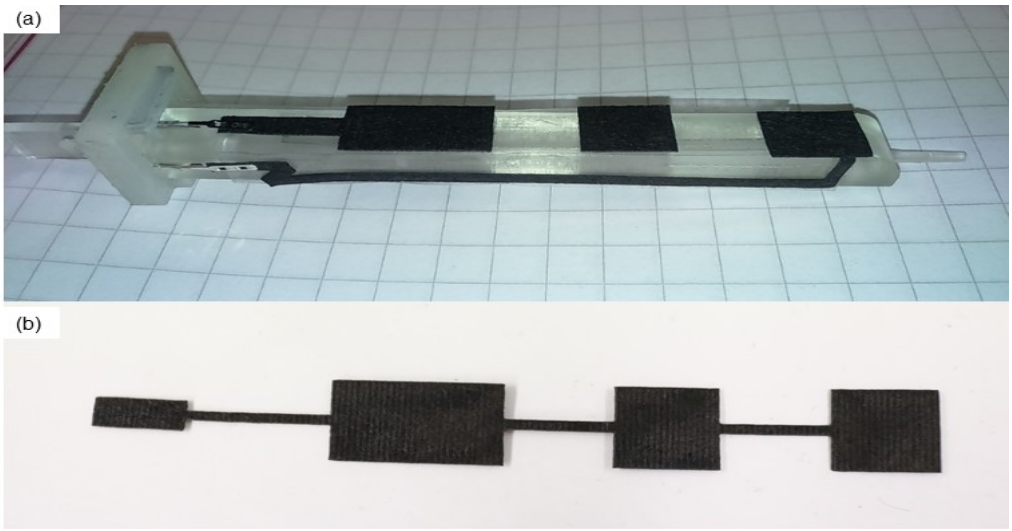

Figure 30. *a) The alignment of lower electrode pads on top of one piece finger, b) upper electrode*

Metallic pins were clamped to the conductive fabric electrodes and wires were soldered to the metallic pins. The metallic pins were wrapped by heat shrink tubing to guarantee isolation of electrodes. Finally, the finger skeleton was inserted inside the skin (Figure 31).

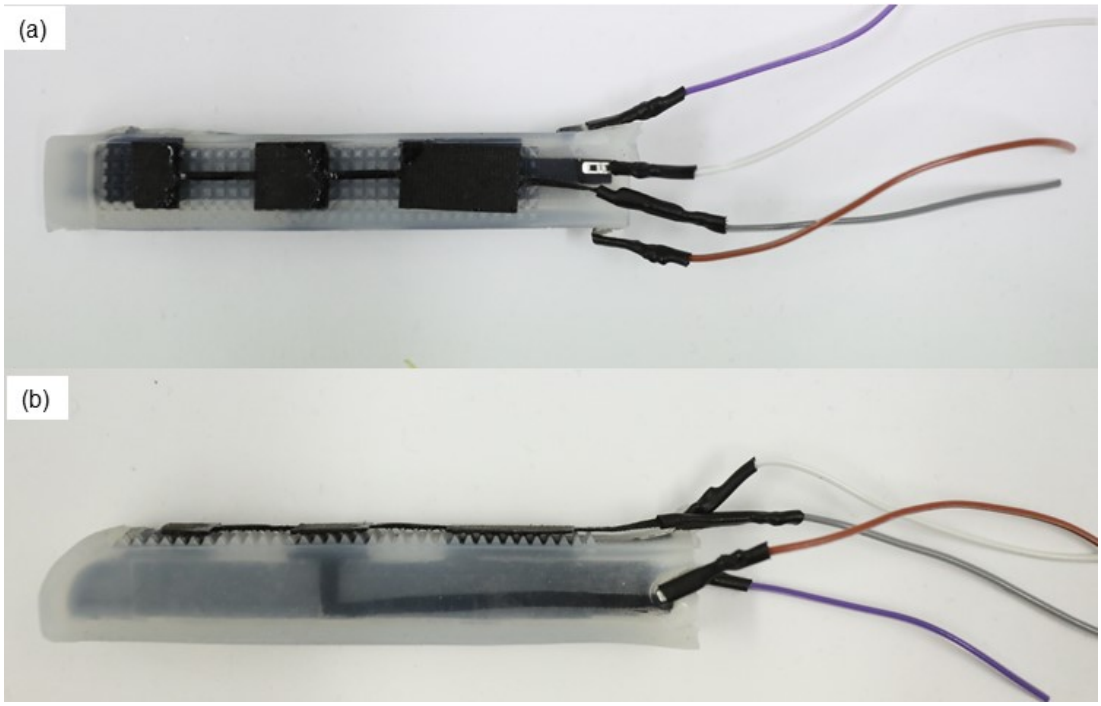

Figure 31. *Final integration of the sensitive artificial skin with the artificial finger skeleton. a) Top view, b) Side view*

6. METHODS FOR CHARACTERIZING SENSORS

This chapter describes the experimental setup for characterizing both sensor types. TA.XT plus Texture Analyser (StableMicroSystems, U.K.) [55] (Figure 32a) was used to apply a known force on the sensor pads. Capacitance was recorded using a precision LCR meter (ST2827A, Sourcetronics, Germany) [56] (Figure 32b), while resistance was recorded using a multifunction data acquisition board (USB-6356, National Instruments, U.S.A) [57] (Figure 32c). MATLAB® software (MathWorks, U.S.A) [58] was used to acquire and process data from the sensors. We will now explain the sensor characterization setup in more detail.

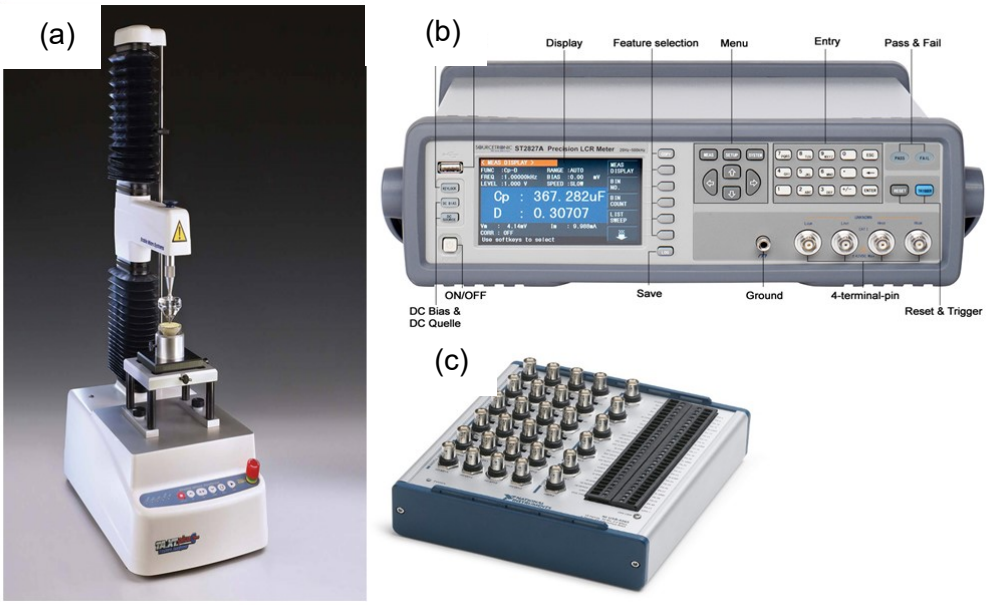

Figure 32. *All tools utilized in characterization: (a)TA.XT plus Texture Analyser* [55]*, (b) Precision LCR meter ST2827A* [56] *and (c) NI USB-6356 multifunction Data Acquisition (DAQ)* [57]

6.1 Experimental setup for characterizing the piezoresistive sensors

To measure the resistance of the piezoresistive sensor, we used a voltage-divider circuit (Figure 33). The sensor was connected in series with a passive sensor, and the variation of the voltage over the passive sensor was recorded. Probes of the data acquisition board (USB-6356, National Instruments) are connected to the terminals of the passive sensor. The data acquisition board was connected to a computer using USB, and Matlab was used to record the data, with a sampling rate of 100 Hz.

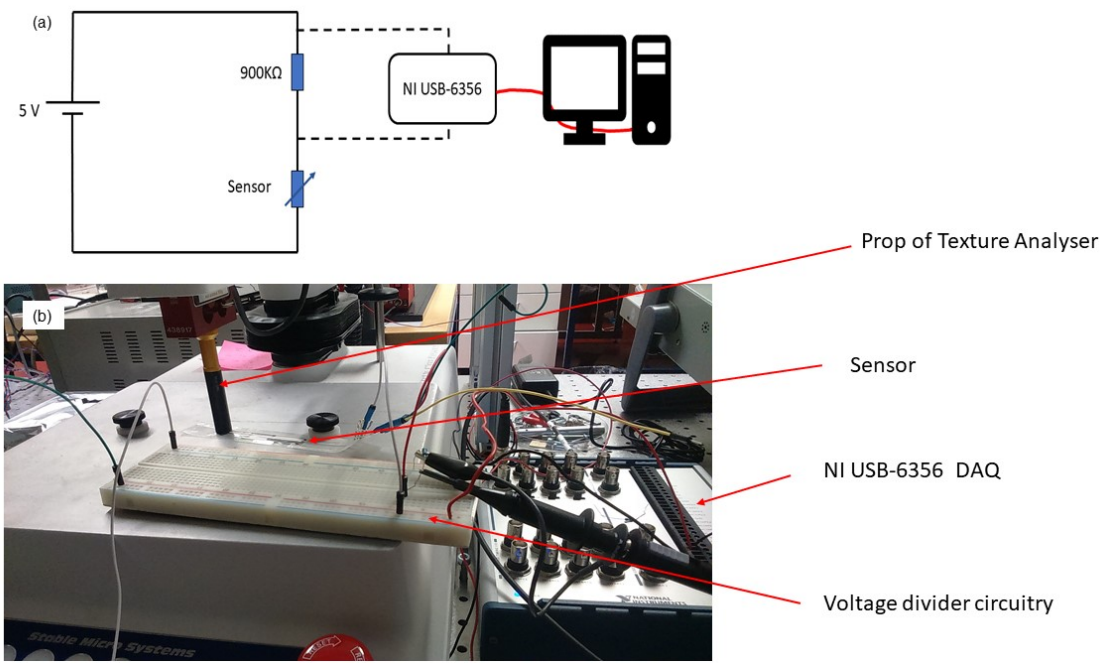

Figure 33. *(a) Schematic of the circuit configuration and (b) the setup to acquire data from the piezoresistive sensor through configuration to NI USB-6356 (DAQ)*

The data acquisition board was recording the voltage across the passive resistor. However, the target was to capture the variation in the resistance of the sensor. For a voltage-divider circuit, the following formula can be derived:

$$R_s = 900\ \text{k}\Omega \left(\frac{V_s}{V_o} - 1\right) \tag{6}$$

where R_s is the resistance of the sensor in kΩ, V_s is the supply voltage that is kept at constant 5 V, and V_o is the voltage across the passive resistor which was equal to 900 kΩ. Equation 6 was used in Matlab® to convert the recorded voltage into resistance.

6.2 Experimental setup for characterizing the capacitive sensors

To acquire the capacitance variation in real-time, the LCR meter (ST2827A, Sourcetronics, Germany) is used as it is shown in Figure 34a. RS-232 is used to communicate with the LCR meter. The capacitive sensor is connected to the LCR meter through a signal cord with alligator clips (Figure 34b).

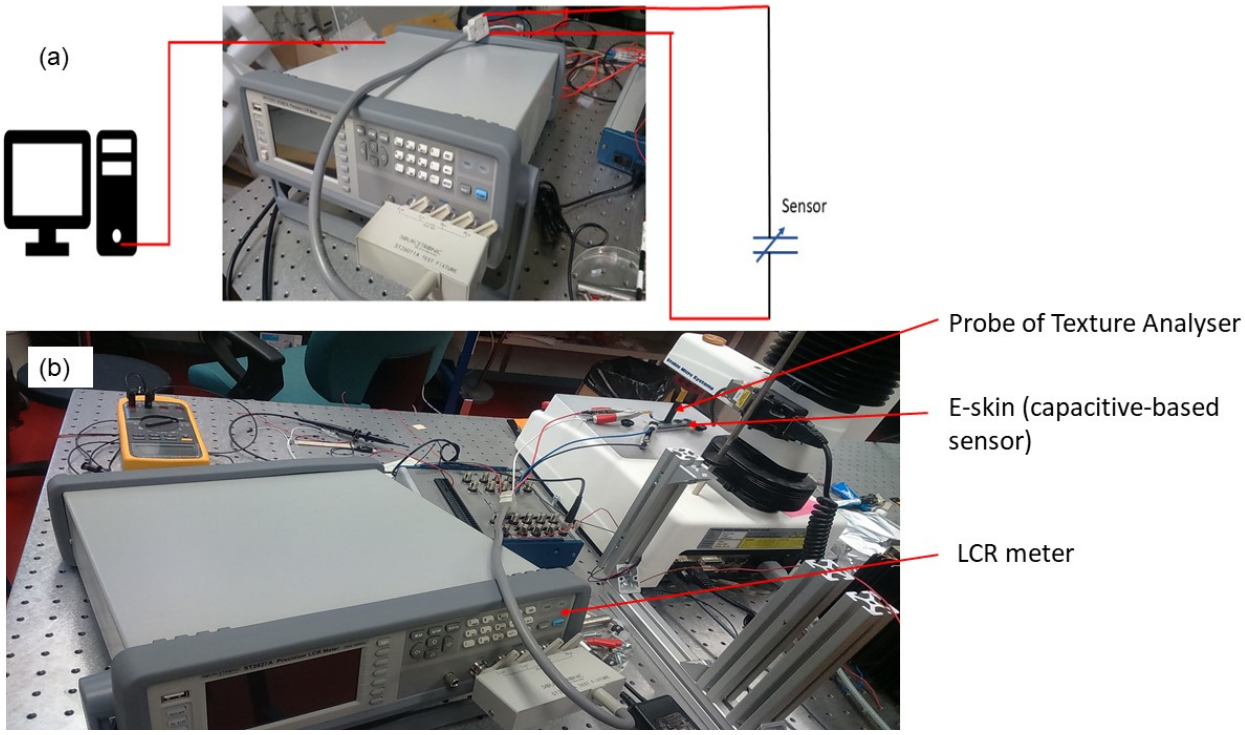

Figure 34. *(a) Schematic configuration of the capacitive sensor and (b) the setup to acquire data from e-skin through configuration to LCR meter*

In all characterization schemas for the capacitive sensor, the LCR meter is adjusted to acquire data every 0.1 seconds because the maximum frequency of input during dynamic loading tests was 2 Hz. To clarify, according to the *Nyquist* sampling theorem, the continuous signal can be properly sampled if the sampling frequency is at least twice the frequency of the input signal [49]. Accordingly, a sampling rate of 10 Hz that corresponds to 0.1 seconds was adequate for our application. The voltage level in the LCR meter is set to 1 V and internal frequency is set to 1 KHz frequency.

6.3 Experimental setup for applying forces on the sensors

During the characterization experiments, the texture analyzer was used to apply force on both sensor types sensors. The sensors were positioned on the stage of the texture analyser stage (Figure 33b) ExponentLite® software on the workstation was used to program the texture analyzer. Using this approach enabled data acquisition in real-time during the exertion of different load patterns by the texture analyzer. To apply the force on the piezoresistive sensors, a cylindrical probe with a diameter of 5 mm was used, while for the capacitive sensors, a cylindrical probe with a diameter of 10 mm was used. The reason for this was that the area of the piezoresistive sensors was smaller than the area of the capacitive sensors.

7. CHARACTERIZATION RESULTS

In this chapter, we report the characterization experiments and results of the fabricated sensors. We will report the key-parameters of these sensors: linearity, viscoelastic-based hysteresis, signal hysteresis, drift, SNR, stability at loaded and unloaded states. Finally, we will compare the merits and demerits of each sensor type.

7.1 Sensitivity and linearity

To measure the sensitivity and linearity of the sensors, the texture analyser was programmed to apply an incremental load on the sensors within a range from 0 to 490 g. The load cell of the texture analyser can withstand a maximum load of 500 g, so 490 g was chosen because of safety concerns. As shown in Figure 35, there was a period of unloading status consecutive to each loading cycle, which would give an indication about the efficiency of recovery to the original state in each sensor type.

Figure 35a shows the resistance versus time for the piezoresistive sensor, and Figure 35b shows the capacitance versus time for the capacitive sensor. Notice how the piezoresistive sensor can easily detect even 10 g load, while the 50 g load is barely noticeable in the capacitive sensor (Figure 35b). Thus, the piezoresistive sensor has a better limit of detection than the capacitive sensor. It is clear from the data that it would be difficult to distinguish the signal from noise at loads lower than 50 g with the capacitive sensor.

Another observable phenomenon in Figure 35 is the recovery of both sensors when no load is applied. The capacitive sensor exhibited higher stability and better recovery in comparison to the piezoresistive sensor. It is also noticeable the piezoresistive sensor overshoots in the instantaneous release of load, which is absent in case of the capacitive sensor.

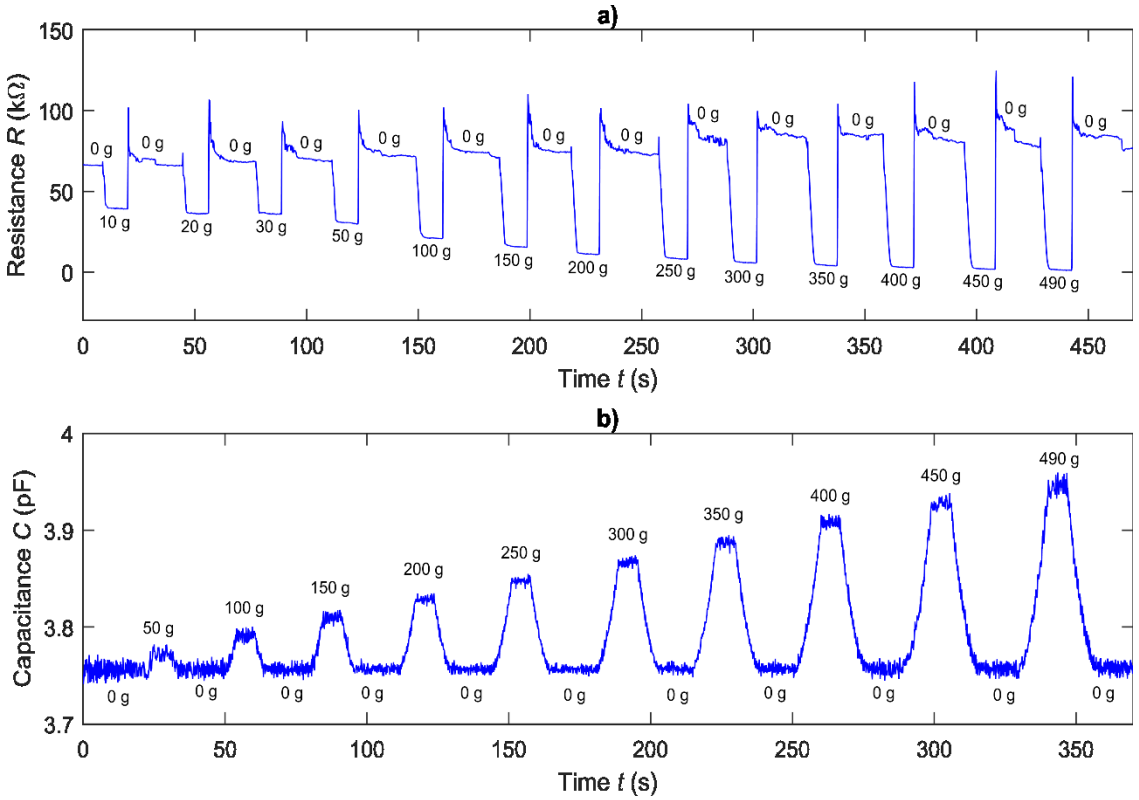

Figure 35. *The incremental increase of loading on the sensor by a texture analyser. (a) Piezoresistive sensor. (b) Capacitive sensor.*

From the data in Figure 35, we can get the relation of resistance or capacitance to applied load (Figure 36). While the piezoresistive sensor showed a non-linear response to the applied load on the sensor by maximum deviation up to 35% from linearity (Figure 36a), the capacitive sensor exhibited a highly linear response to the load applied on it (Figure 36c), with a maximum deviation of 1.8% from linearity. The relative change in resistance (Figure 36a) is much higher than the relative change in capacitance (Figure 36c). The relative resistivity of the piezoresistive sensor changed in from 0 to almost -1, which means almost -100% of change from the intrinsic resistivity of the sensor at load variation from 0 of 490 g. The capacitive sensor changed in the range from 0 to 0.045, which mean 4.5 % change from the intrinsic capacitance of the sensor under the same loading range.

Linear regression is applied within the MATLAB platform to get the best mathematical model, which express the characteristics of both sensors. In the case of the capacitive sensor, we get the following fitted equation:

$$C\ [\mathrm{pF}] = 0.0004\ m\ [\mathrm{g}] + 3.75, \tag{8}$$

where *m* is the load. Conversely, the piezoresistive sensor is not well-approximated by a linear equation. However, by plotting the sensor response on a logarithmic y-scale (log

R vs. *m*), we get a nice linear relation, as shown in Figure 36b. The maximum deviation from linearity in the logarithmic scale is only 5.3%. Consequently, it became feasible to apply linear regression technique to find the best fitting mathematical model for this sensor response:

$$R\ [\mathrm{k\Omega}] = e^{-0.007\ m\ [\mathrm{g}] + 3.79}, \tag{9}$$

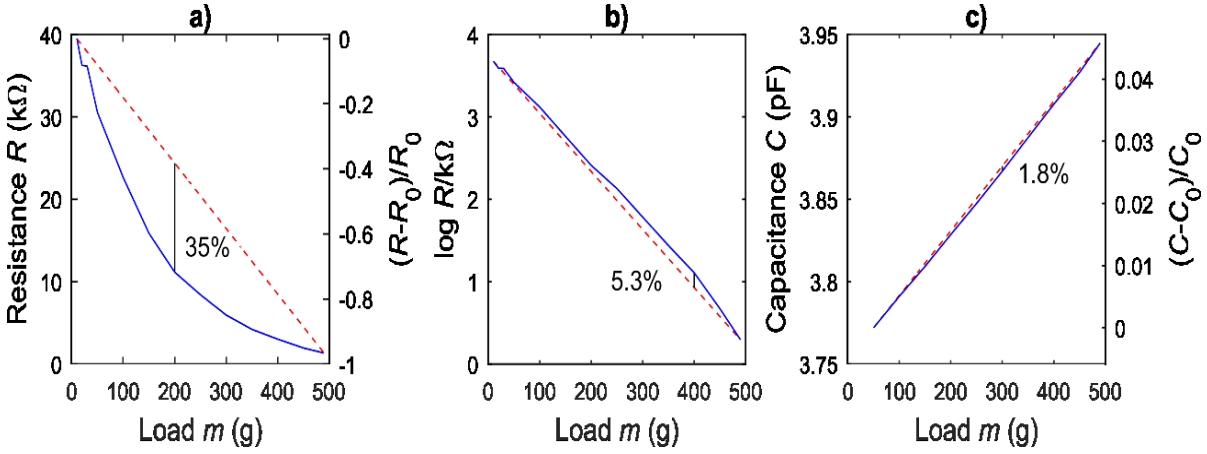

Figure 36. *Characterizing sensitivity and linearity for (a) resistance of piezoresistive sensor versus load with 35% deviation from linearity, (b) Variation of resistance of piezoresistive sensor versus load in logarithmic scale with 5.3% deviation from linearity, (c) Variation of capacitance versus load in the capacitive type sensor with 1.8% deviation from linearity.*

7.2 Viscoelasticity

On high-frequency applications such as the utilization of the robotic hand in the industry for gripping mobile objects on a conveyor belt that moves swiftly, the response of the sensor should be fast. The response speed of the sensor is limited partly by the viscoelasticity of the sensor material. Viscoelasticity of material gives an indication of the response speed of the sensor when the material is squeezed under the effect of mechanical stimuli. In both sensors, the acquired signal is derived directly from the variation of the distance between the upper and lower electrode, so any viscoelasticity of this layer will delay the response of the sensor.

To measure the viscoelastic properties of both sensors, sinusoidal load with 6 different frequencies were applied on both sensors by the texture analyser (Figure 37). Both sensors show quite similar viscoelasticity. As the frequency of applied load is increasing in the range from 0.1Hz to the maximum of 2Hz, the sensor started to exhibit higher relative hysteresis. Nevertheless, a distinguishable feature between the two sensors was the difference in displacement which can be induced in the sensor for the same magnitude

of applied load on both sensors. For a load of 250 g, the piezoresistive and the capacitive sensors displaced 70 um and 350 µm, respectively.

These results show clearly that both sensors are not suitable for high-frequency applications, because they display already significant phase-lag at 1 Hz. In other words, if the objective is to use the robotic hand in high-speed process (e.g. production line, to sort objects rapidly with high frequent signal acquisition from sensory apparatus), it will be enough to recognize the gripping of targeted object; however, the detailed information about the magnitude of load exerted on the sensory apparatus during object grasping will be imprecise.

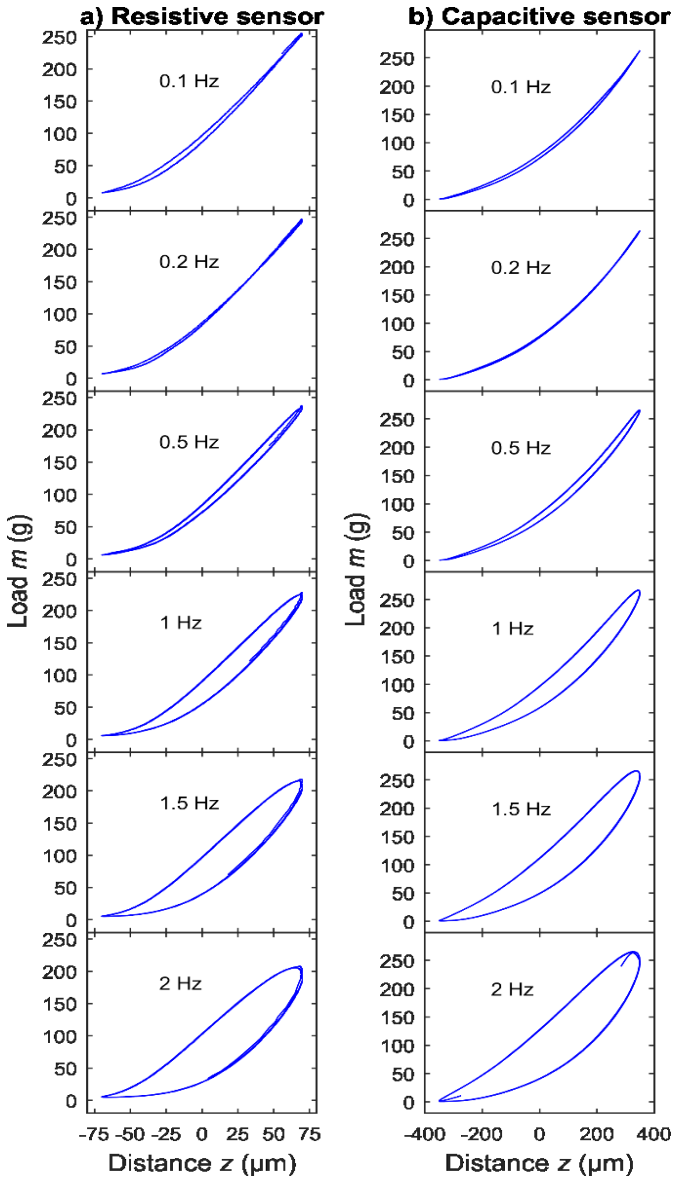

Figure 37. *Viscoelastic-based hysteresis under the effect of cyclic pressure with different frequencies of 0.1 Hz, 0.2 Hz, 0.5 Hz, 1 Hz, 1.5 Hz, and 2 Hz for (a) piezoresistive sensor, (b) Capacitive sensor*

7.3 Hysteresis

Signal hysteresis is an undesirable phenomenon, which results in different output for the same magnitude of input when it affects from a different direction. In Figure 37, we saw no hysteresis in the material due to viscoelasticity when 0.1 Hz loading was applied. Figure 38 shows the recorded sensor signals corresponding to this 0.1 Hz loading, by plotting log *R* vs. *m* and *C* vs. *m*.

The capacitive sensor was noisy but exhibited very little hysteresis, ~ 2.7% after filtering (Figure 38b). In comparison, the piezoresistive sensor exhibited a higher range of hysteresis up to 18.2% (Figure 38a). The estimated amount of hysteresis in the capacitive sensor is close to the noise level so it is difficult to distinguish even so small capacitance from the noise (Figure 38b). Despite that both sensors showing almost the same level of viscoelastic-based hysteresis, the capacitive sensor showed better performance in terms of sensor signal hysteresis. The hysteresis and creep are well-known disadvantages of force-sensing resistors [10].

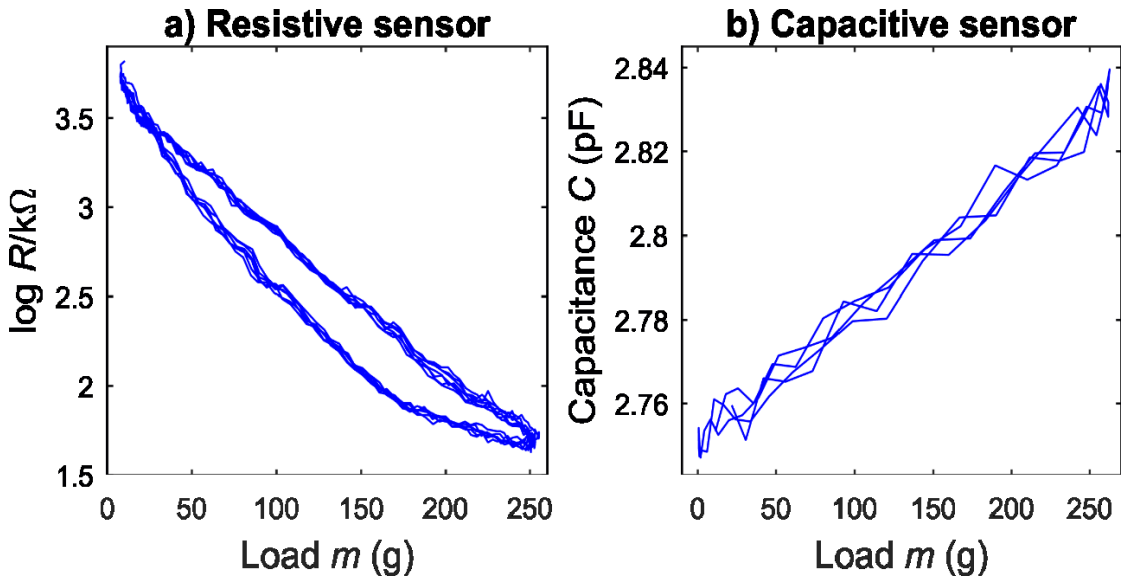

Figure 38. *Comparing signal hysteresis under the effect of 0.1 Hz sinusoidal pressure applied by Texture Analyzer on a) piezoresistive sensor, (b) Capacitive sensor.*

7.4 Drift

Drift is one of the key-parameters defining sensor efficiency. With drift, we mean the stability of sensor signal under constant load. Drift is expressed as the fractional ratio between the maximum variation in the output signal to the time corresponding to this variation, while a constant load is applied on the sensor. A lower value of the drift is

better. In addition to static load, we were interested in the stability of the sensor signal under cyclic load, which we call dynamic stability.

To estimate drift and dynamic stability, we applied a sinusoidal load with 1 Hz frequency for 200 cycles, and then a static load of 90 g for at least 30 minutes. The results for both sensor types are shown in Figure 39.

At the initiation of the static load application, the capacitance of capacitive sensor was 3.54 pF and the resistance of the piezoresistive sensor was 19.1 kΩ. After 30 min, the sensors showed values of 3.5397 pF and 16.7 kΩ, respectively. By calculating the relative drift in both sensors, the capacitive sensor has a lower relative drift of 0.52%, while the piezoresistive sensor has a higher drift of 4.3%.

Figure 39b compares the stability of the two sensors in cyclic loading. The piezoresistive sensor showed a noticeable gradual decrease in the output due to the creep effect, another typical property of resistive sensor with silver-based electrodes [10]. In comparison, the capacitive sensor signal remained considerably more stable without overshooting or creep effect since the initiation of dynamic loading test until the last cycle in the test.

In conclusion, the result indicates that the capacitive type sensor is more stable than the piezoresistive sensor.

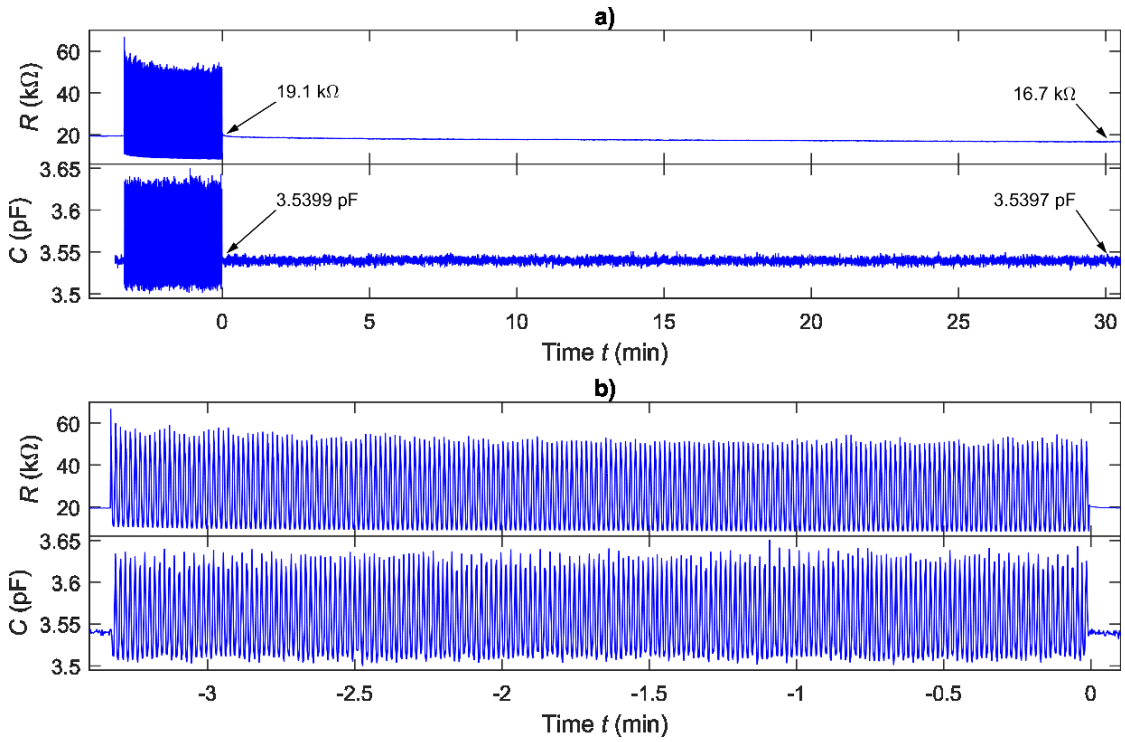

Figure 39. *Comparing both of piezoresistive and capacitive sensor performance in terms of (a) drift estimation, (b) repeatability observation; Testing under dynamic load (1 Hz sinusoidal loading) followed by static load fixed at 90 g.*

7.5 No-load stability and SNR

A typical problem with tactile pressure sensors is that they display large fluctuations in the sensor signal when no load is applied. Figure 40 compares the no-load stability performance for both sensors by first applying a static load of 90 g by texture analyser and then swiftly removing the load. In the case of the piezoresistive sensor (Figure 40a), there was significant overshoot immediately after removing the load, followed by minor fluctuations of the sensor signal for several minutes after the removal of the load. In the case of the capacitive sensor (Figure 40b), there were no noticeable fluctuations in the output, except the variation in the output due to noise.

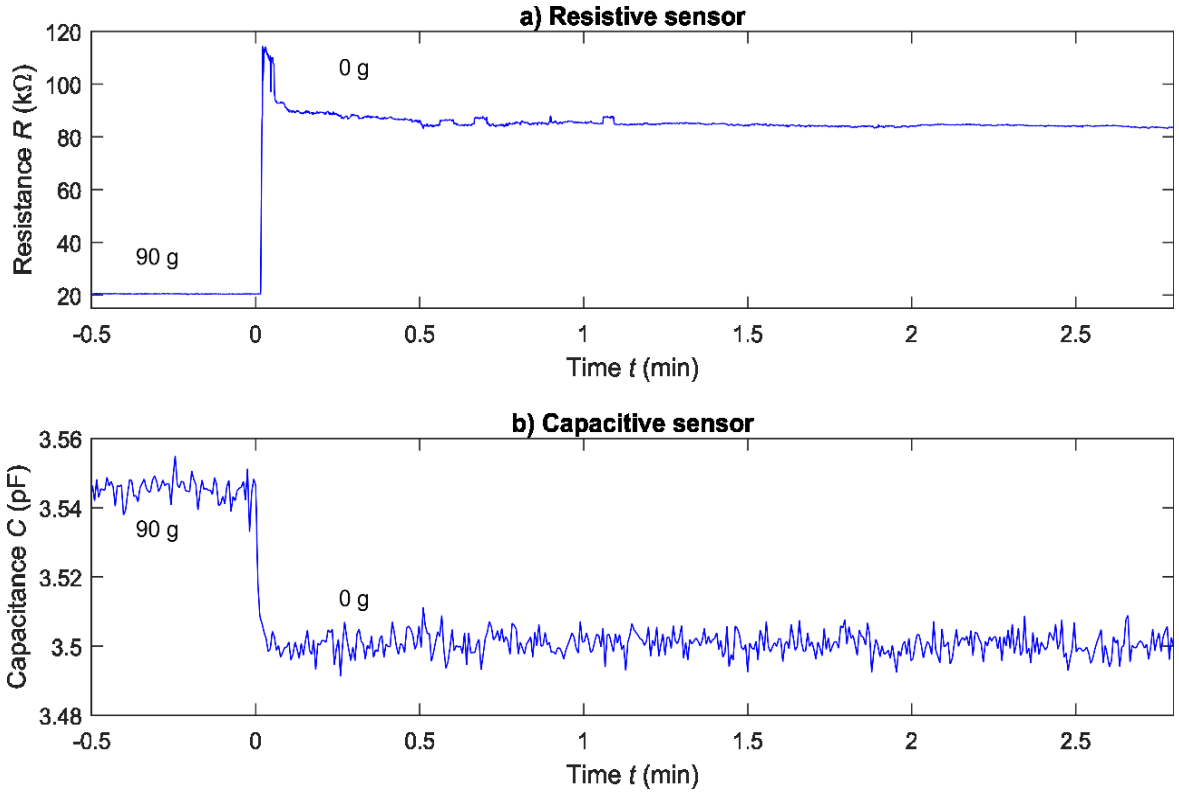

Figure 40. *Comparing the no-load stability for (a) piezoresistive sensor, (b) capacitive sensor; by application of 90 g static load and removal to 0 g, then, recording the no-load variation for around 3 minutes*

From these step response experiments, we can also infer the signal-to-noise ratio (SNR). We calculated SNR using the following formula: [49]

$$\mathrm{SNR} = 20\log_{10}\frac{|\bar{x}_{\mathrm{loaded}} - \bar{x}_{\mathrm{unloaded}}|}{\sigma_{\mathrm{unloaded}}}, \tag{10}$$

where $\bar{x}$ denotes the mean of a signal and σ denotes the standard deviation. Using this formulat, SNR is found to be 52 dB and 24 dB for the piezoresistive and capacitive sensors, respectively. The piezoresistive sensor possessed higher SNR than the capacitive sensor.

7.6 Comparing the performance of the two sensors

Table 4 summarizes all characterization results for both types of sensors. In general, the comparison shows the superiority of the capacitive sensor. However, the only demerit of the capacitive sensor was the lower SNR in comparison with its counterpart in case of piezoresistive sensor. Nevertheless, the lower SNR of the capacitive sensor is derived from the design of the sensor that reported in this thesis. Based on what is reported in the literature, still better results could be obtained for the capacitive sensor, by adjusting the fabrication process. This will be further discussed in the Chapter “Discussion”.

Table 4. *Comparing the performance of both Capacitive and Piezoresistive sensor*

Parameter	Piezoresistive sensor	Capacitive sensor	Key-parameter evaluation
Linearity	5.3% (on log-R scale)	1.8%	Smaller is better
Viscoelasticity @ 0.1 Hz	4.2%	2.7%	Smaller is better
Viscoelasticity @ 2 Hz	37.1%	34.4%	Smaller is better
Sensor signal hysteresis @ 0.1 Hz	18.2%	2.7%	Smaller is better
Drift	4.3 %	0.52 %	Smaller is better
SNR	52 dB	24 dB	Larger is better

7.7 Demonstration of the capacitive sensor integrated into the SRH

The main goal of this thesis is to fabricate an artificial skin with a sensitivity to touch for a robotic hand. Based on the results summarized in Table 4, it was decided to demonstrate the capacitive sensors integrated into a robotic hand. The capacitive sensors, integrated into the SRH, are shown in Figure 41.

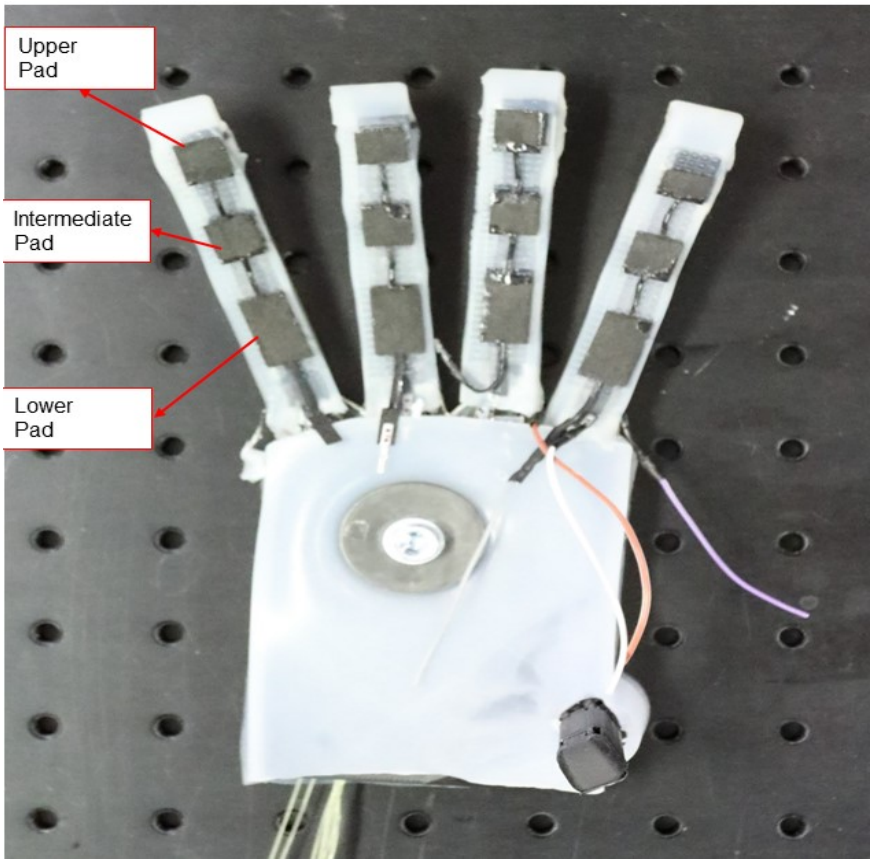

Figure 41. *The robotic hand with e-skin in the final phase. Each finger has three sensitive partitions: upper pad, intermediate pad and lower pad*

Ideally, the tactile pressure sensors would be only sensitive to contact force and would show no response to bending of the fingers. Figure 42 shows the sensor response of the sensors when the fingers are bent and unbent. The capacitance recorded while fingers were activated for around 60 seconds followed by deactivation for 30 seconds. The hand fingers were activated and deactivated by pulling and releasing the tendons that extended in hollow channels embedded in the hand structure.

Significant changes in the capacitance can be observed due to bending. This is most likely due to the change in distance between the upper and lower electrode owing to the strain induced in the elastomeric skin during finger bending. It is also obvious that the response of the three pads for the same e-skin was dissimilar. To clarify, the results reveal the heterogeneity in the level of strain across the e-skin surface, where it is obvious that the intermediate partition of the e-skin was the most susceptible section for textural variation during hand actuation, as it can be noticed from the repetitive pattern of intermediate pad measurements in all fingers. On the other hand, the upper pad exhibited the lowest variation under the impact of finger actuation in all tested cases.

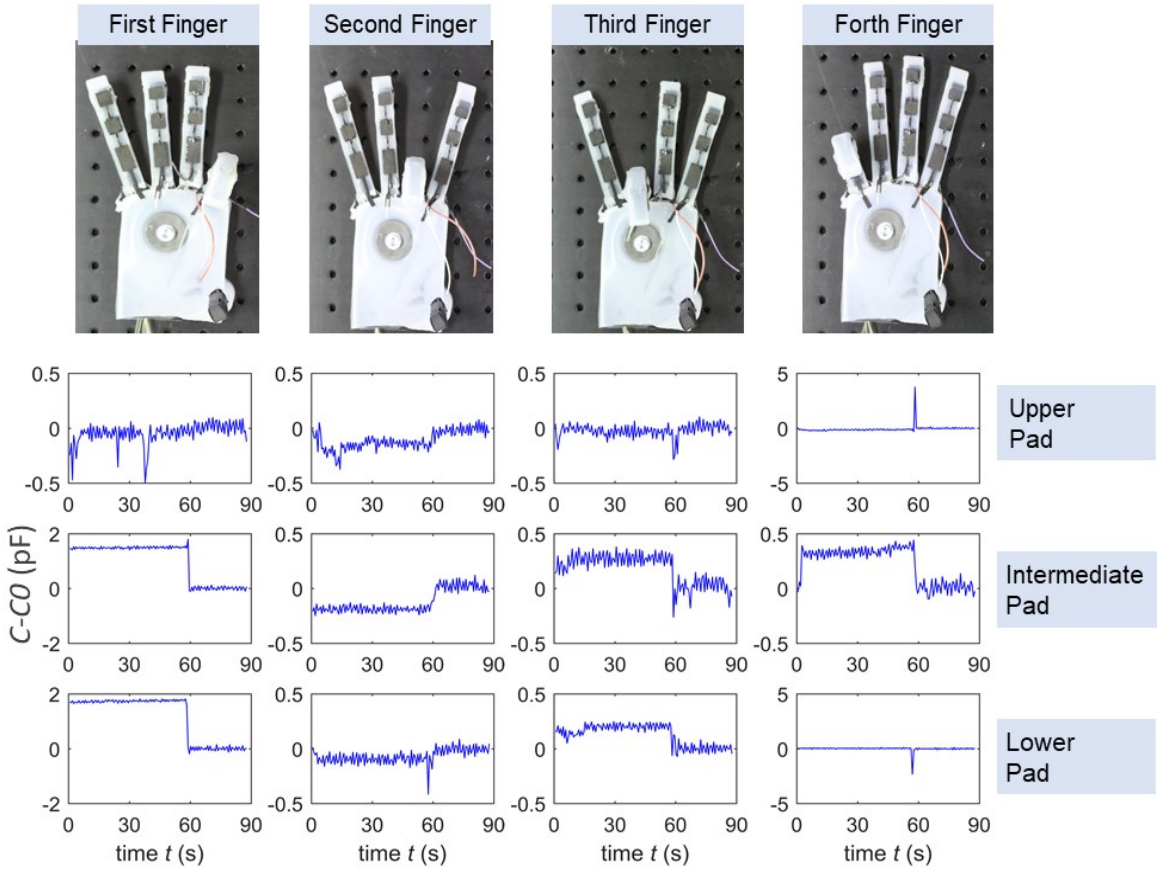

Figure 42. *The variation in capacitance of the e-skin during fingers actuation. Each finger is activated for 1 minute by pulling the tendons that extended in hallow channels embedded inside the hand and deactivated sequentially for 30 seconds by releasing the driving tendons*

Furthermore, there is some level of asymmetry in the acquired patterns from different fingers for the same corresponding pads. This can render to fabrication issues such as some deficiencies in the elastomer, a small level of deviation in the alignment between sensor pads and the centroid of the geometry of finger phalanges. Generally, the inconsistency in the readings between fingers can be explained in terms of dissimilarity of the e-skin associated with each finger.

8. CONCLUSIONS AND DISCUSSIONS

The objective of this work was to propose a solution for robotic grippers inspired by the human hand in terms of dexterous manipulation, soft touch and sensation capabilities. As a result, The proposed robotic hand can be utilized as a prosthetics or elaborated in the industry as a soft robotic hand with sense of touch. To achieve this objective, there were challenges that brought up the following research questions.

The first question was about finding a suitable technique that allows fast reconfigurability and promoting the democratization of producing this sort of grippers either for industrial or biomedical purposes. To fulfill this target, we demonstrated utilization of rapid prototyping approach based on 3D printing, laser cutting and elastomer casting. With the continuous improvement in these technologies and the affordability of a wide range of processable materials, it became possible to print 3-dimensional objects with different levels of complexity, mechanical and chemical properties. In this thesis, we utilized both of FDM and SLA printer to fabricate the artificial skeleton of the hand and the mold, which used for artificial skin casting, as well as, the mold for a structured dielectric layer of the capacitive sensor.

The second research question was about selecting two sensors for further investigation through fabrication and characterization. After studying comparatively the sensor technologies, we decided to proceed with a piezoresistive sensor and a capacitive sensor; driven by the need for an easy, simple, low-cost and compliance with attributes of the artificial skin. The two sensors are fabricated and characterized comparatively to find that the capacitive sensor is generally outperforming the piezoresistive sensor, as shown in Table 4. Moreover, the capacitive sensor had a higher potential for integration with the artificial skin to form an e-skin.

The proposal in this thesis offers simple, direct, robust, conformal structure and low-cost solution for the fabrication of capacitive e-skin. The characterization results showed also the capability of e-skin in acquiring a pressure tactile information from the SRH.

Despite the interesting results that we get for the capacitive e-skin, there is room for improvement. For instance, minimizing the thickness of the dielectric layer between the upper and lower electrodes of the capacitive sensor to increase the intrinsic capacitance. Reducing the size of electrode pads and aligning it with the centroid of finger phalanges to minimize the effect of the strain induced in the skin during finger bending that leads to

the interference with pressure tactile signal. Altering the geometry of the replica mold and using more elastic skin, to increase the sensitivity of the skin and enhancing the SNR, by allowing higher compressibility for the dielectric layer. Tackling these issues would result in enhancing the overall performance.

Accordingly, the results pave the way for further improvement in the domain of humanoid robots by using e-skin with robotic grippers to achieve a dexterous control over objects gripping or granting the ability of objects recognition. Dexterous gripping for the targeted objects is realizable by integrating the sensitive SRH into a closed control loop system. Moreover, the progress in this domain can be beneficial for producing prosthetic hands with real-time sensory feedback.

REFERENCES

[1] Z. Huichan, O. Kevin, L. Shuo, and S. Robert, “Optoelectronically innervated soft prosthetic hand via stretchable optical waveguides,” *Sci. Robot.*, vol. 1, no. 1, 2016.

[2] C. Melchiorri, G. Palli, G. Berselli, and G. Vassura, “Development of the UB hand IV: Overview of design solutions and enabling technologies,” *IEEE Robot. Autom. Mag.*, vol. 20, no. 3, pp. 72–81, 2013.

[3] Y. Wan, Y. Wang, and C. F. Guo, “Recent progresses on flexible tactile sensors,” *Mater. Today Phys.*, vol. 1, pp. 61–73, 2017.

[4] “Soft Robotics.” [Online]. Available: https://www.softroboticsinc.com/food-beverage. [Accessed: 02-Jun-2019].

[5] “New Hampshire Public Radio.” [Online]. Available: https://www.nhpr.org/post/nh-vet-becomes-first-fitted-two-luke-arms#stream/0. [Accessed: 17-May-2019].

[6] “Mobius Bionics.” [Online]. Available: http://www.mobiusbionics.com/. [Accessed: 17-May-2019].

[7] M. A. Lebedev and M. A. L. Nicolelis, “Brain-machine interfaces: past, present and future,” *Trends Neurosci.*, vol. 29, no. 9, pp. 536–546, 2006.

[8] M. Raspopovic *et al.*, “Restoring Natural Sensory Feedback in Real-Time Bidirectional Hand Prostheses,” *Sci. Transl. Med.*, vol. 6, no. 222, pp. 222ra19-222ra19, 2014.

[9] P. Marasco *et al.*, “Illusory movement perception improves motor control for prosthetic hands,” *Sci. Transl. Med*, vol. 10 (432), 2018.

[10] A. Koivikko, E. S. Raei, M. Mosallaei, M. Mäntysalo, and V. Sariola, “Screen-printed curvature sensors for soft robots,” *IEEE Sens. J.*, vol. 18, no. 1, pp. 223–230, 2018.

[11] R. S. Dahiya and M. Valle, *Robotic Tactile Sensing*. Dordrecht: Springer Netherlands, 2013.

[12] S. Kang *et al.*, “Highly Sensitive Pressure Sensor Based on Bioinspired Porous Structure for Real-Time Tactile Sensing,” *Adv. Electron. Mater.*, vol. 2, no. 12, 2016.

[13] T. Morita, H. Iwata, and S. Sugano, “Development of human symbiotic robot: WENDY,” in *Proceedings 1999 IEEE International Conference on Robotics and Automation*, vol. 4, pp. 3183–3188.

[14] R. O. Ambrose *et al.*, “Robonaut: NASA’s space humanoid,” *IEEE Intell. Syst.*, vol. 15, no. 4, pp. 57–63, Jul. 2000.

[15] C. S. Lovchik and M. A. Diftler, “The Robonaut hand: a dexterous robot hand for

space," in *Proceedings 1999 IEEE International Conference on Robotics and Automation (Cat. No.99CH36288C)*, vol. 2, pp. 907–912.

[16] M. T. Mason and J. K. Salisbury, *Robot hands and the mechanics of manipulation*. MIT Press, 1985.

[17] G. Wöhlke, "A programming and simulation environment for the karlsruhe dextrous hand," *Rob. Auton. Syst.*, vol. 6, no. 3, pp. 243–263, Jul. 1990.

[18] W. Jongkind, "Dextrous gripping in a hazardous environment: guidelines, fault tolerance and control," in *Proceedings of IEEE Systems Man and Cybernetics Conference - SMC*, pp. 509–514.

[19] A. Weigl and M. Seitz, "Vision assisted disassembly using a dexterous hand-arm-system: An example and experimental results," *IFAC Proc. Vol.*, vol. 27, no. 14, pp. 315–320, Sep. 1994.

[20] "Jacobsen, Steve C., et al. 'The UTAH/MIT dextrous hand: Work in progress.' The International Journal of Robotics Research 3.4 (1984): 21-50."

[21] J. M. Ochoa, Yicheng Jia, D. Narasimhan, and D. G. Kamper, "Development of a portable actuated orthotic glove to facilitate gross extension of the digits for therapeutic training after stroke," in *2009 Annual International Conference of the IEEE Engineering in Medicine and Biology Society*, 2009, pp. 6918–6921.

[22] R. J. Sanchez *et al.*, "A Pneumatic Robot for Re-Training Arm Movement after Stroke: Rationale and Mechanical Design," in *9th International Conference on Rehabilitation Robotics, 2005. ICORR 2005.*, pp. 500–504.

[23] Mark E. Rosheim, *Robot Evolution: The Development of Anthrobotics*. New York: John Wiley & Sons, Inc., 1994.

[24] G. Hirzinger *et al.*, "A mechatronics approach to the design of light-weight arms and multifingered hands," in *Proceedings 2000 ICRA. Millennium Conference. IEEE International Conference on Robotics and Automation. Symposia Proceedings (Cat. No.00CH37065)*, vol. 1, pp. 46–54.

[25] F. Lotti and G. Vassura, "A novel approach to mechanical design of articulated fingers for robotic hands," in *IEEE/RSJ International Conference on Intelligent Robots and System*, vol. 2, pp. 1687–1692.

[26] R. Noorani, *3D Printing : Technology, Applications, and Selection*. CRC Press, 2017.

[27] "All 10 Types of 3D Printing Technology in 2019 | All3DP." [Online]. Available: https://all3dp.com/1/types-of-3d-printers-3d-printing-technology/. [Accessed: 04-Jun-2019].

[28] "High Resolution SLA and SLS 3D Printers for Professionals | Formlabs." [Online]. Available: https://formlabs.com/. [Accessed: 04-Jun-2019].

[29] J. L. Pons, *Emerging actuator technologies : a micromechatronic approach*. Wiley, 2005.

[30] D. Rus and M. T. Tolley, "Design, fabrication and control of soft robots," *Nature*,

vol. 521, no. 7553, pp. 467–475, 2015.

[31] A. Atieh, “Spatial resolution inhand,” Concordia University, 2012.

[32] “Smooth-On, Inc.” [Online]. Available: https://www.smooth-on.com/. [Accessed: 02-Apr-2019].

[33] S. A. Boppart, “Biomechanical Properties of In Vivo Human Skin From Dynamic Optical Coherence Elastography,” *IEEE Trans. Biomed. Eng.*, vol. 57, no. 4, pp. 953–959, 2010.

[34] “Measuring Strain with Strain Gages - National Instruments.” [Online]. Available: http://www.ni.com/fi-fi/innovations/white-papers/07/measuring-strain-with-strain-gages.html. [Accessed: 25-Apr-2019].

[35] Alamusi, N. Hu, H. Fukunaga, S. Atobe, Y. Liu, and J. Li, “Piezoresistive strain sensors made from carbon nanotubes based polymer nanocomposites,” *Sensors*, vol. 11, no. 11, pp. 10691–10723, 2011.

[36] J. S. Kim and G. W. Kim, “Hysteresis compensation of piezoresistive carbon nanotube/polydimethylsiloxane composite-based force sensors,” *Sensors (Switzerland)*, vol. 17, no. 2, 2017.

[37] K. Chu, D. Kim, Y. Sohn, S. Lee, C. Moon, and S. Park, “Electrical and Thermal Properties of Carbon-Nanotube Composite for Flexible Electric Heating-Unit Applications,” *IEEE Electron Device Lett.*, vol. 34, no. 5, pp. 668–670, May 2013.

[38] H. J. M. T. S. Adriaens, W. L. De Koning, and R. Banning, “Modeling piezoelectric actuators,” *IEEE/ASME Trans. Mechatronics*, vol. 5, no. 4, pp. 331–341, 2000.

[39] T. R. Kuphaldt, “Lessons In Electric Circuits, Volume I – DC,” *October*, 2006. [Online]. Available: allaboutcircuits.com.

[40] C. To, T. Hellebrekers, J. Jung, S. J. Yoon, and Y. L. Park, “A Soft Optical Waveguide Coupled with Fiber Optics for Dynamic Pressure and Strain Sensing,” *IEEE Robot. Autom. Lett.*, vol. 3, no. 4, pp. 3821–3827, 2018.

[41] “Capacitive sensors versus inductive sensors - Zettlex.” [Online]. Available: https://www.zettlex.com/articles/a-comparison-of-inductive-and-capacitive-position-sensors/. [Accessed: 10-Apr-2019].

[42] S. Garain, S. Jana, T. K. Sinha, and D. Mandal, “Design of In Situ Poled Ce^{3+} -Doped Electrospun PVDF/Graphene Composite Nanofibers for Fabrication of Nanopressure Sensor and Ultrasensitive Acoustic Nanogenerator,” *ACS Appl. Mater. Interfaces*, vol. 8, no. 7, pp. 4532–4540, Feb. 2016.

[43] Z. Ming, X. Ruan, C. Bao, Q. Lin, Y. Yang, and L. Zhu, “Micropatterned Protein for Cell Adhesion through Phototriggered Charge Change in a Polyvinylpyrrolidone Hydrogel,” *Adv. Funct. Mater.*, vol. 27, no. 25, p. 1606258, Jul. 2017.

[44] S. C. B. Mannsfeld *et al.*, “Highly sensitive flexible pressure sensors with microstructured rubber dielectric layers,” *Nat. Mater.*, vol. 9, no. 10, pp. 859–864, 2010.

[45] L. Ma *et al.*, “A highly sensitive and flexible capacitive pressure sensor based on

a micro-arrayed polydimethylsiloxane dielectric layer," *J. Mater. Chem. C*, vol. 6, no. 48, pp. 13232–13240, 2018.

[46] Y. Wan *et al.*, " Ionic Skin with Biomimetic Dielectric Layer Templated from Calathea Zebrine Leaf ," *Adv. Funct. Mater.*, vol. 28, no. 37, p. 1802343, 2018.

[47] R. Mancini, *Op Amps For Everyone*. Texas Instruments, 2002.

[48] "Electrical noise and mitigation." [Online]. Available: https://www.eetimes.com/document.asp?doc_id=1274125&page_number=1. [Accessed: 29-Apr-2019].

[49] W. Strauss, "Digital signal processing," *IEEE Signal Process. Mag.*, vol. 17, no. 2, pp. 52–56, Mar. 2000.

[50] "Active Low Pass Filter - Op-amp Low Pass FilterBasic Electronics Tutorials." [Online]. Available: https://www.electronics-tutorials.ws/filter/filter_5.html. [Accessed: 21-May-2019].

[51] J. A. Maxwell *et al.*, *Foundations of Analog and Digital Electronic Circuits*, vol. 5, no. 3rd. 2009.

[52] K. Madhavan Nampoothiri, N. R. Nair, and R. P. John, "An overview of the recent developments in polylactide (PLA) research," *Bioresour. Technol.*, vol. 101, no. 22, pp. 8493–8501, Nov. 2010.

[53] T. D. Sheet, "CI-1036, Highly Conductive & Highly Flexible Silver Ink, Technical Data Sheet," *ECM Tech. Data Sheet*, no. 740, pp. 5–6, 2010.

[54] "ADAFRUIT ADA1364 | Knit Jersey Conductive Fabric - 20c | yeint.fi." [Online]. Available: https://www.yeint.fi/en/electronics/development-tools/wearable-electronics/knit-jersey-conductive-fabric-20c. [Accessed: 06-Mar-2019].

[55] "Stable Micro Systems." [Online]. Available: https://www.stablemicrosystems.com/index.html. [Accessed: 22-Jun-2019].

[56] "Precision LCR Meter ST2827A." [Online]. Available: https://www.sourcetronic.com/shop/en/precision-lcr-meter-st2827a-300khz.html. [Accessed: 22-Jun-2019].

[57] "NI USB-6356 - National Instruments." [Online]. Available: http://sine.ni.com/nips/cds/view/p/lang/fi/nid/209075. [Accessed: 22-Jun-2019].

[58] "MathWorks - Makers of MATLAB and Simulink." [Online]. Available: https://www.mathworks.com/. [Accessed: 22-Jun-2019].